International Journal of Robotics and Control Systems
Vol. 4, No. 3, 2024, pp. 1158-1185
ISSN 2775-2658
http://pubs2.ascee.org/index.php/ijrcs

A Novel Predictive Voltage Control Technique for a Grid Connected Five Phase Permanent Magnet Synchronous Generator

Hussein Mahmoud [a,b,1], Mohamed A. Mohamed [b,2], Ahmed A. Hassan [b,3], Mahmoud A. Mossa [b,4,*]

[a] Electrical Engineering Department, Faculty of Engineering, Damietta University, Damietta 34517, Egypt
[b] Electrical Engineering Department, Faculty of Engineering, Minia University, Minia 61111, Egypt
[1] h_mahmoud777@du.edu.eg; [2] dr.mohamed.abdelaziz@mu.edu.eg; [3] ahmed.hasan@mu.edu.eg;
[4] mahmoud_a_mossa@mu.edu.eg
* Corresponding Author

ARTICLE INFO

Article history
Received April 08, 2024
Revised June 14, 2024
Accepted July 06, 2024

Keywords
Five-Phase PMSG;
Wind Turbine;
MPPT;
Vector Control;
Predictive Control;

ABSTRACT

This study focuses on developing an effective control strategy to enhance the dynamics of a wind turbine grid-connected five-phase permanent magnet synchronous generator (PMSG). To visualize the superior performance of the newly proposed controller, the generator's performance is evaluated with another traditional predictive control scheme: predictive torque control (PTC). However, the vector control principle is applied to the GSC converter. The PTC has limitations such as significant ripple, substantial load commutation, and the inclusion of a weighting element in its cost functions. The proposed predictive methodology aims to overcome limitations, uses a simple cost function, and doesn't require weighting elements to address concerns about stability errors. Comparing the proposed predictive voltage controller (PVC) to the PTC, the findings show that the suggested PVC has many benefits, including faster dynamic response, a simpler control structure, fewer ripples, reduced current harmonics, low computation burdens, and robustness, so the generated power affects system efficiency, leading to improved power quality and reduced switching losses, enhancing power converters efficiency and their switches lifespan, this fact is verified mathematically as the total harmonic distortion (THD) has reduced to 1.346% average percentage for the proposed controller. However, the THD of the PTC is 3.05%. In addition, the study examines the incorporation of pitch angle control (PAC) and maximum power point tracking (MPPT). These controls restrict the consumption of wind energy when the generator speed surpasses its rated speed and optimize the extraction of wind energy during periods of low wind availability. In summary, the proposed PVC-enhanced control system reveals superior performance in dynamic response, control simplicity, current quality, and computational efficiency compared to other methods.

1. Introduction

Recently, an ongoing decrease in the available conventional fuel and environmental issues has increased the requirement for renewable energy alternatives that may be harnessed with minimal environmental impact [1]-[3]. These energy sources can be found in various forms such as

geothermal, biomass, hydro, wind, wave, and solar energies [4], [5]. However, renewable energies have some advantages such as the absence of carbon dioxide and other greenhouse gases that do not affect the environment, reliability, natural replenishment, accessibility, and cleanliness. Still, they require proper sizing and management to achieve optimal utilization [4], [6]. Thus, each of these elements plays a part in why wind energy has been selected as the most important use of renewable energy [7]. The Global Wind Energy Council Outlook 2012 states that 282,430 MW of total wind power was generated globally in 2012 [8]. The cleanest and most environmentally friendly renewable energy source is wind energy, which is produced by air currents moving across the surface of the earth, and they use this air's kinetic energy to generate electricity [9], [10]. An appropriate generation system is necessary to capture the most amount of power from the wind for variable speeds [8].

Wind turbines can run at rates that are fixed or variable. Increased energy extraction, operation at the point of greatest power, increased efficiency, and higher power quality are simply a few benefits that variable-speed wind turbines (VSWT) have over fixed-speed wind turbines (FSWT) [11]. Otherwise, asynchronous generators operating on a connection to a grid are easier to operate with FSWT, and they are cheaper because they don't require power converters [12]. VSWTs' robust energy output offsets their expensive initial cost. VSWT provides several advantages, such as the ability to increase or decrease the speed of the wind turbine. The tower, gearbox, and other drive train sections will experience less wear and tension. Variable-speed devices increase energy output and create more power by maintaining an ideal TSR ratio. As a result, the power coefficient Cp remains at its greatest value, whereas Ptp maintains a cubic connection with wind speed when compared to fixed speed types. Wind-driven generators frequently need blade angle and MPPT controls. This also reduces power injection fluctuations into the grid [11]. These factors contribute to selecting a variable-speed wind turbine.

Wind generation systems including FSWT or VSWT employ a variety of machine types [13]. The squirrel-cage induction generator (SCIG) requires an external source of reactive power to excite the machine [14], [15]. The doubly fed induction generator (DFIG) offers control flexibility from the rotor side, using a converter with lower capacity to reduce cost [16]-[18].DFIG has several advantages, such as handling high-power ratings [19], operating at FSWT or VSWT with lower-scale power converters [20], [21], supplying reactive power, and operating fault-tolerant [18], [19]. However, it also has shortcomings like poor power factors, low efficiency, increased maintenance due to slip rings, and requirement for Rotor excitation current [22], [23]. Improvements are needed to enhance reliability.

The ongoing research targets permanent-magnet synchronous generators (PMSGs) because of their self-excitation feature, which enables high power factor and efficiency and has attracted a lot of interest in wind energy applications [24], [25]. In addition, compared to asynchronous machines, PMSG possesses several benefits including high-efficiency [26], lightweight, enhanced power density, and ease of operation [27], [28]. Researchers are more interested in replacing traditional three-phase PMSG with multi-phase generators to overcome limitations, enhance power density, and shrink the converter's size, as well as utilize low-grade switching devices [29], [30]. Multi-phase permanent-magnet synchronous machines offer excellent reliability, the lower amplitude of torque pulsation with better power density segmentation which distributes loads across a variety of components [31], inferior rotor harmonic current, reduction in phase current without raising the phase voltage, and lower ripples of DC bus current [32], [33], these machines are flexible in faulted conditions meaning they can continue to operate even if one or two phases are faulty [34]-[36]. The five-phase PMSG is a more effective multi-phase generator compared to multi-phase induction machines [37], [38].

Generators may be controlled using a variety of control techniques, but one of the trickiest aspects of the generating system is determining which control is best. For regulating the dynamics of five-phase PMSG, many control algorithms are being studied. the authors in [39], [40] used the vector control approach to maintain a steady DC-bus voltage and to accomplish a decoupled regulation of the direct and quadrature components of generated current, allowing them to deliver

the most active power to the grid. Furthermore, the reactive power by the wind energy conversion system (WECS) is adjusted to follow zero. Although good steady-state performance was attained, there was poor dynamic in the system response with overshoot [41], [42]. Furthermore, PI current regulators require precise tuning, which may increase the complexity and reduce the system's efficiency [43], [44]. In [45] the researchers adopted direct torque control (DTC), which uses a distinctive switching table and two hysteresis comparators. This control scheme offered a quicker dynamic response than vector control but resulted in visible ripples and current harmonics. Subsequently, modern control techniques such as sliding mode control (SMC) and model predictive control (MPC) were adopted. SMC was found to be effective in regulating five-phase PMSG's dynamics [46], [47] but resulted in increased system complexity and chattering effects [48]. Integral sliding mode control (ISMC) was then developed to eliminate steady-state errors [49], and a high-order sliding mode controller was used to address the chattering phenomenon [50], [51].

Predictive control (PC) has recently been adopted and superseded traditional control systems due to its ability to overcome the limitations of conventional control topologies [52]. Predictive control (PC) has different configurations such as finite control set (FCS), continuous control set, hysteresis-based, and trajectory-based [53], [54]. The FCS MPC exhibits the most encouraging characteristics among these classifications due to its utilization of switching states instead of PWM [54], [55]. For these reasons, various predictive controllers implement the FCS principle. In references [56], [57] predictive power control (PPC) employs a similar approach to a conventional DPC based on a lookup table. However, the hysteresis comparators and lookup table databases were replaced by a solitary cost function (C_f) that amalgamated the absolute errors of the machine powers. Also, in reference [58] the predictive torque control (PTC) is based on the cost function linked to the torque and flux absolute errors. When comparing these two predictive controls to the traditional DPC and DTC, the performance of PMSG was enhanced in ripples reduction, however, the complexity of both controllers was noticeable. In addition, they require a weighting factor (ω_f) in their cost function. ω_f is used to compensate for each control variable concerning others [59]. The PTC has various defects, including a greater computation burden owing to estimating and predicting torque and flux values in the cost function. This requires a powerful microprocessor for this defect [60]. Long sample intervals and low switching frequency might increase torque ripple and reduce stator current quality when employing the weighting factor.

Prior to this thorough review, our goal was to create an efficient control system that would meet these requirements while avoiding the shortcomings of the conventional PTC method. To that end, the current study attempts to develop a predictive control technique that limits commutation losses and yields superior performance, such as quick dynamic response in comparison to sliding mode control, low ripple in comparison to model predictive torque and model predictive power controllers, and robustness against parameter variation in comparison to DTC, FOC, and other traditional predictive controllers. introduces the design of an efficient predictive controller that uses a comparable cost function made up of similar components (the stator voltage d-q-x-y components) and does not require the use of a weighting factor, the rippling effects resulting from incorrect weighting value detection are mitigated by using the cost function.

According to this review, the paper's contributions are delineated as follows:

1. Introduce and model a WECS-based wind turbine for five-phase PMSG.
2. The pitch angle control (PAC) and maximum power point tracking (MPPT) are used to achieve the best power under various environmental circumstances.
3. The practicality of the contemplated generation method has been validated for changes in wind speed.
4. The paper introduced a detailed design of the control of both machine-side converter (MSC) and grid-side converter (GSC).

5. An innovative predictive voltage control approach (PVC) has been introduced to improve the dynamics of synchronous generators.
6. The stability function of Lyapunov is used to analyze the proposed PVC applied to the MSC.
7. The paper presents a flow chart of the two predictive control methods.
8. A detailed comparison of the two predictive controller PTC, and the proposed PVC is accomplished to outline the performance improvements.

The paper is organized in the following manner: The modeling of WECS, including wind turbine as well as its PAC and MPPT, five-phase PMSG, generator, grid converters, DC bus, and filter design are described in Section 2, whereas Section 3 outlines GSC, and MSC control systems, including the proposed design. The performance evaluation results are shown in Section 4. Lastly, the conclusions are summed up in Section 5.

2. System Under Study

2.1. Wind Generation System Modeling

Fig. 1 shows the system that is being studied. The wind generation system consists of a wind turbine, a five-phase PMSG, and a five-phase rectifier at the generator side which is linked to a three-phase inverter on the grid side, each with its control unit. This system is connected to the utility grid through the grid side converter (GSC) and filter. The control system is utilized for each component to optimize their performance. The wind turbine applies MPPT and PAC to extract the maximum wind energy, the generator converter is regulated by predictive control to improve its dynamics, and the grid converter is controlled by vector control. Moreover, it is essential for the system to integrate the MSC, which necessitates control to effectively regulate the energy delivered power from it to a grid. We assessed the dynamic performance of the generator for this system using various control techniques to determine which one operated the best. This included evaluating the suggested predictive voltage. To validate these assertions, a comprehensive mathematical model for each system unit must be provided.

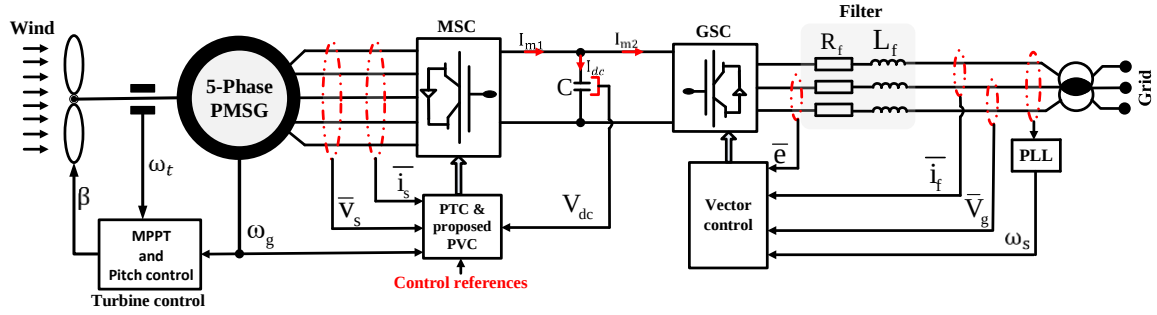

Fig. 1. The wind generation system under-study

2.1.1. Turbine Modeling

Aerodynamic power is converted to mechanical power on the wind turbine-generator shaft depending on the radius of the blade, the velocity of the wind, and the power coefficient. A turbine model is necessary for Simulation. PAC is implemented by selecting an appropriate angle (β). The MPPT is applied to harvest the maximum available energy from the turbine for wind speeds lower than nominal. PAC and MPPT will be explained briefly. The tip speed ratio (λ) is illustrated as follows [61]:

$$\lambda = \frac{RW_t}{V_w} \tag{1}$$

Where R is the radius of the blade.

The power coefficient (Cp) that manages and regulates the amount of electricity generated by wind. To get Cp for given λt and β, the power coefficient relies on bitch angle (β) and tip ratio speed (λt). For this purpose, the following formulas have been applied. The power coefficient is determined as follows [62], [63].

$$Cp(\lambda,\beta) = 0.53\left(\frac{151}{\lambda_i} - 0.58\beta - 0.002\beta^{2.14} - 10\right)e^{\frac{-18.4}{\lambda_i}} \quad (2)$$

Where

$$\lambda_i = \frac{1}{\frac{1}{\lambda - 0.02\beta} - \frac{0.003}{\beta^3 + 1}} \quad (3)$$

The wind power and the turbine power (P_w, P_t) are:

$$P_w = 0.5\rho A V_W^3 \text{ and } P_t = 0.5\rho A C_p V_W^3 \quad (4)$$

Where (ρ) indicates specified air density. From Equations (1), (2), and (3), the turbine torque T_t is calculated by:

$$T_t = \frac{P_t}{\omega_t} = \frac{0.5\rho A C_p V_W^3}{\omega_t} \quad (5)$$

To achieve a balance between the turbine and generator shaft, a serious need for a gearbox ratio has to be met, so we can clarify the generator torque (T_g) and the generator speed (ω_m)as follows:

$$T_g = \frac{T_t}{K} \text{ and } \omega_g = K\omega_t \quad (6)$$

Where K is the gear ratio.

The mechanical dynamic equation of the WECS is illustrated at the instant KT_s and a sample time of T_s as shown:

$$T_{t,(k)} - KT_{g,(k)} - DK\omega_{t,(k)} = \left(\frac{J_t}{K} + KJ_g\right)\frac{d\omega_{t,(k)}}{dt} \quad (7)$$

Where J_t and J_g are the inertia of the turbine and generator, and D is the friction coefficient.

The target is to implement the MPPT to harvest the maximum energy from the wind, which can be achieved when the turbine is at C_{p_Max} (i.e. at C_{p_Opt}). Thus, it is imperative to maintain the rotor speed at the tip speed ratio (TSR) λ_{Opt} optimal value. The rotor speed needs to be modified to match any fluctuations in wind speed. Thus, the optimal power of the wind turbine can be written as:

$$P_{t\_Opt} = 0.5\rho A C_{p\_Opt}\left(\frac{\frac{R\omega_m}{K}}{\lambda_{Opt}}\right)^3 \quad (8)$$

Therefore, the turbine and generator optimum torque is:

$$T_{t\_Opt} = \frac{P_{t\_Opt}}{\omega_t} \text{ and } T_{g\_Opt} = \frac{T_{t\_Opt}}{K} \quad (9)$$

The power coefficient (C_{p_opt}) is maximized when the PMSG velocity can be controlled to maintain the optimal difference speed ratio (λopt) during wind velocity fluctuations. This indicates

that the turbine system has reached maximum power. Fig. 2 illustrates the relation between C_p and λ for distinct pitch angle (β) values and clearly shows that C_{p_max} occurs when the TSR achieves its peak value, and β is zero [55].

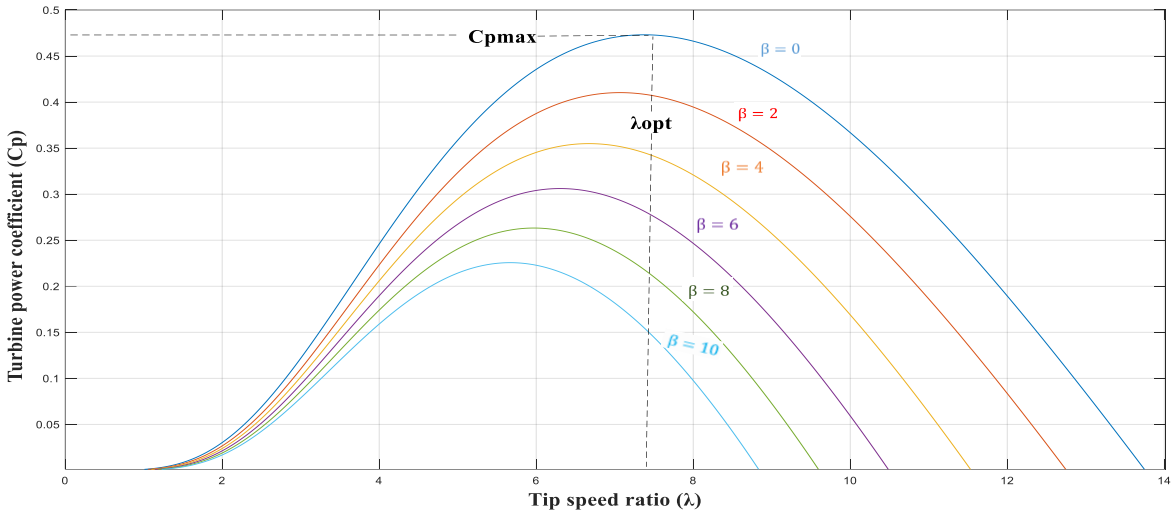

Fig. 2. Relationship between C_p and TSR for different β values

The purpose of using PAC is to keep the machine operating at its rated output power regardless of whether the wind speed goes above it. The pitch angle is typically adjusted to zero degrees in the MPPT zone and triggered in the torque region and it is controlled by tracking the wind speed and selecting an appropriate angle (β) based on the ($V_w - \beta$) curve as shown in Fig. 3. The proportional-integral (PI) controller uses β to regulate the generator output power to the rated amount. When the pitch angle rises, Cp decreases along with the extracted wind power (see (4)), while the generator power recovers to its rated value.

The methodology of using a PAC is first from the look-up table the pitch angle is selected according to the wind speed then the angle is compared to the actual pitch angle and the error is adjusted by using PI controller which is responsible for producing the most electricity from available wind.

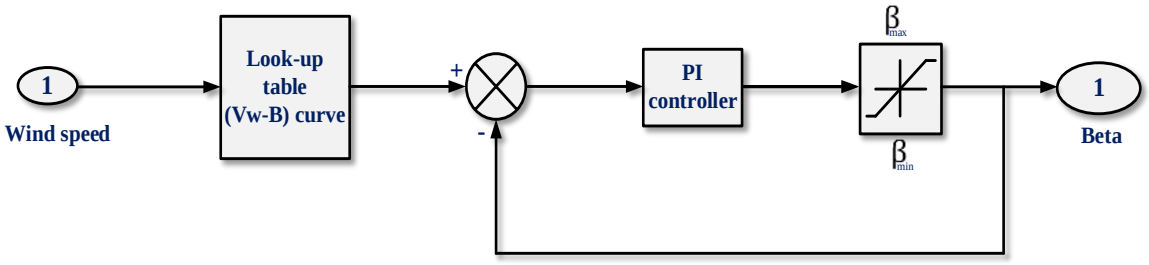

Fig. 3. Block diagram of pitch angle controller

Fig. 4 depicts the wind turbine's operational zone in detail; in the region (1) the wind speed is below its cut-in value so no power would be produced. the MPPT is operated at region (2) only when wind speed is less than the rated value but greater than the cut-in value. The pitch angle is set to zero. Typically, PAC is activated in the torque region (3). The MPPT is a technique to catch maximum power for any given wind. It should be noted that in the region (4) since there is a significant rise in wind speed, the structure will be unable to impact PAC, and will thus shut down [64].

2.1.2. Five-Phase PMSG Model

A five-phase Permanent Magnet Synchronous Generator (PMSG) is a complex machine that provides better performance than standard three-phase PMSGs. They require a more intricate

mathematical model and advanced control strategies [65].However, it is often utilized in variable wind speed turbines because of the benefits discussed before [66]. One advantage is the absence of an excitation circuit in the rotor, which eliminates the requirement for slip rings.

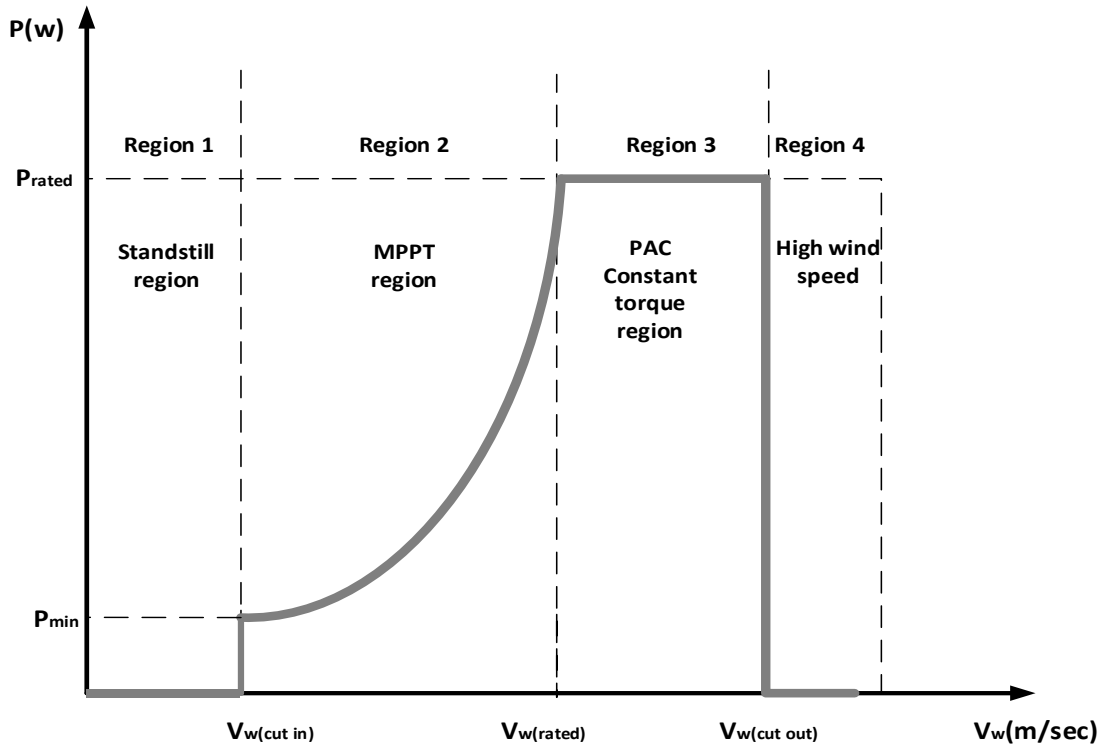

Fig. 4. Operational zone of a wind turbine

The electric model of the five-phase PMSG can be expressed by using a rotating (d-q-x-y) synchronous frame at the instant KT_s by using sampling time Ts as follows [67].

$$\frac{di_{ds,(k)}}{dt} = \frac{1}{L_s}\left[V_{ds,(k)} - R_s i_{ds,(k)} + pL_s\omega_{g(k)} i_{qs,(k)}\right] \tag{10}$$

$$\frac{di_{qs,(k)}}{dt} = \frac{1}{L_s}\left[V_{qs,(k)} - R_s i_{qs,(k)} - pL_s\omega_{g,(k)}\left(i_{ds,(k)} + \frac{\varphi_f}{L_s}\right)\right] \tag{11}$$

$$\frac{di_{xs,(k)}}{dt} = \frac{1}{L_l}V_{xs,(k)} - \frac{R_s}{L_l}i_{xs,(k)} \tag{12}$$

$$\frac{di_{xs,(k)}}{dt} = \frac{1}{L_l}V_{xs,(k)} - \frac{R_s}{L_l}i_{xs,(k)} \tag{13}$$

Where the parameters R_s, L_s, and L_l indicate the stator resistance, inductance, and leakage inductance, p is the pair of poles, ω_g is the generator shaft speed, and φ_f is the permanent magnet flux.

Using the permanent magnet, flux linkage and stator current components, the generated encounter torque may be expressed analytically as follows:

$$T_{g,(k)} = \frac{5}{2}pI_m\left(\varphi_{ds,(k)} - j\varphi_{qs,(k)}\right)\left(i_{ds,(k)} + ji_{qs,(k)}\right) \tag{14}$$

$$+\left(\varphi_{xs,(k)}-j\varphi_{ys,(k)}\right)\left(i_{xs,(k)}+ji_{ys,(k)}\right)$$

$$=\frac{5}{2}p\left(\varphi_{ds,(k)}i_{qs,(k)}-\varphi_{qs,(k)}i_{ds,(k)}+\varphi_{xs,(k)}i_{ys,(k)}-\varphi_{ys,(k)}i_{xs,(k)}\right)$$

To mitigate the losses of the machine and third harmonic current, the component of the machine current i_{ds}, i_{dx}, i_{dy} are oriented to zero, so the machine torque is expressed by:

$$T_{g,(k)}=\frac{5}{2}p(\varphi_f i_{qs,(k)}) \tag{15}$$

2.2. Machine-Side Converter (MSC) Model

As shown in Fig. 1 a five-phase converter manages the power produced by the five-phase PMSG [68]. The converter's switching states are:

$$S_{abcde,(k)}=[S_{a,(k)}\quad S_{b,(k)}\quad S_{c,(k)}\quad S_{d,(k)}\quad S_{e,(k)}]^T\in\{0,1\}^5 \tag{16}$$

If $S_{i,(k)}=1$ for $i\in\{a\quad b\quad c\quad d\quad e\}$, the lower switch has been disabled while the upper one has been activated. Thus, the terminal voltages V_{abcde} of the generator can be calculated as follows:

$$\begin{bmatrix}V_{a,(k)}\\V_{b,(k)}\\V_{c,(k)}\\V_{d,(k)}\\V_{e,(k)}\end{bmatrix}=\frac{V_{dc,k}}{5}\begin{bmatrix}4&-1&-1&-1&-1\\-1&4&-1&-1&-1\\-1&-1&4&-1&-1\\-1&-1&-1&4&-1\\-1&-1&-1&-1&4\end{bmatrix}\begin{bmatrix}S_{a,(k)}\\S_{b,(k)}\\S_{c,(k)}\\S_{d,(k)}\\S_{e,(k)}\end{bmatrix} \tag{17}$$

where $\theta=\frac{2\pi}{5}$.

In Fig. 5, the thirty-two (32) voltage vectors of a five-phase converter are depicted in the α-β plan and w-z plan. Every individual space vector is uniquely identified by the binary switching sequence S_{abcde}. The harmonics of order $(10N\pm3)$ are represented in the w-z space, whereas those of order $(10N\pm1)$-th as (N = 0, 1, 2, 3,...) are denoted in the α-β space.

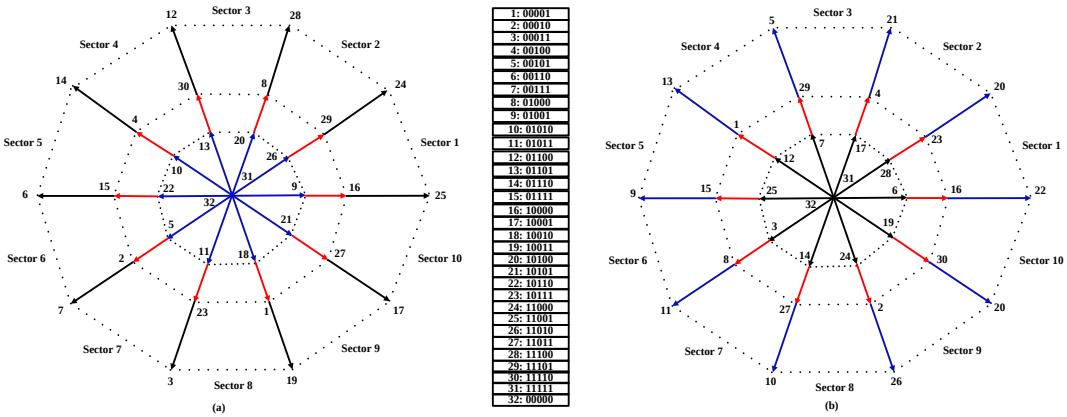

Fig. 5. Vector distribution in α-β frame (a), and in w-z frame (b)

The MSC average model is illustrated as follows:

$$\begin{bmatrix}v_{ds,(k)}\\v_{qs,(k)}\\v_{xs,(k)}\\v_{ys,(k)}\end{bmatrix}=\frac{V_{dc,(k)}}{4}\begin{bmatrix}v^c_{ds,(k)}\\v^c_{qs,(k)}\\v^c_{xs,(k)}\\v^c_{ys,(k)}\end{bmatrix} \tag{18}$$

Where $v^c_{ds,(k)}, v^c_{qs,(k)}, v^c_{xs,(k)}, v^c_{ys,(k)}$ are the control signals that applied to MSC.

Fig. 1 shows the average modulated current $I_{m1,(k)}$ that can be calculated with the help of generator currents components in dqxy frame i_{ds}, i_{qs}, i_{xs}, i_{ys} by:

$$I_{m1,(k)} = 0.75\left(v^c_{ds,(k)} i_{ds,(k)} + v^c_{qs,(k)} i_{qs,(k)} + v^c_{xs,(k)} i_{xs,(k)} + v^c_{ys,(k)} i_{ys,(k)}\right) \quad (19)$$

2.3. Modeling of Grid Side Converter, DC Bus, and Grid Filter

Fig.1 shows that, through an output filter and a GSC, the utility grid is connected to the wind-driven five-phase PMSG. The filter must be designed properly to regulate the DC bus voltage to pass the generated power to the utility grid and achieve a unity power factor [69], [70]. Suppose the grid voltage v_g is centered on the d-axis of a synchronous frame, then.

$$v_{qg,(k)} = \left|\bar{v}_{g,(k)}\right|, \text{ and } v_{dg,(k)} = 0.0 \quad (20)$$

The expression for the voltage equilibrium over the filter is:

$$\frac{di_{df,(k)}}{dt} = \frac{1}{L_f}\left[u_{df,(k)} - R_f i_{df,(k)} + L_f \omega_{s,(k)} i_{qf,(k)}\right] \quad (21)$$

$$\frac{di_{qf,(k)}}{dt} = \frac{1}{L_f}\left[u_{qf,(k)} - R_f i_{qf,(k)} - L_f \omega_{s,(k)} i_{df,(k)} - v_{qg,(k)}\right] \quad (22)$$

Where the filter's resistance and inductance are R_f and L_f , respectively The GSC d-q voltages are $u_{df,(k)}$ and $u_{qf,(k)}$, the grid angular frequency is $\omega_{s,(k)}$, regulated by a PLL system, and the d-q axis current components of the general utility are denoted as $i_{df,(k)}$ and $i_{qf,(k)}$. As equation (18) the voltage average model of three-phase GSC can be calculated as follows:

$$\begin{bmatrix} u_{df,(k)} \\ u_{qf,(k)} \end{bmatrix} = \frac{V_{dc}}{2} \begin{bmatrix} u^c_{df,(k)} \\ u^c_{qf,(k)} \end{bmatrix} \quad (23)$$

Where $u^c_{df,(k)}$ and $u^c_{qf,(k)}$ are the control signals of GSC. As Equation (19). $I_{m2,(k)}$ at the GSC shown in Fig. 1 can be calculated as follows:

$$I_{m2,(k)} = 0.5\left(u^c_{df,(k)} i_{df,(k)} + u^c_{q,(k)} i_{qf,(k)}\right) \quad (24)$$

The dynamic of the DC bus can be determined from (19) and (24) as follows:

$$C\frac{dV_{dc,(k)}}{dt} = I_{m1,(k)} - I_{m2,(k)} = I_{dc,(k)} \quad (25)$$

where C is bus capacitance, $V_{dc,(k)}$ is the DC potential, $I_{dc,(k)}$ is the current through the DC link.

Notably, the designs of the control systems for the MSC and GSC will be elaborated upon in Section 3. The system's specifications are given in Table 1.

After modeling all system components from wind turbine to grid modeling, the following section will explain the design of the control system adopted for both the grid-side converter and machine-side converter.

3. Adopted Control Methods

This section outlines and explicates the precise design procedures pertaining to control systems. The control is implemented in the MSC and GSC. For the GSC, it is controlled by vector control

(VC). On the other hand, the MSC is regulated by two control algorithms: PTC, and the formulated PVC control. This is to investigate and deeply analyze the generator's performance. Fig. 6 simplifies the overall system structure showing the possibility of control type applied to both the MSC and GSC.

Table 1. System's parameters and data specifications

Parameter	Value	Parameter	Value
R	2 m	R_s	0.67 Ω
P_{rated}	3900 W	L_s	3.2 mH
$V_{w,nom}$	10 m/s	φ_f	0.2 T
K	3.8	C	2.2 mF
$2p$	4	T_s	100 µs

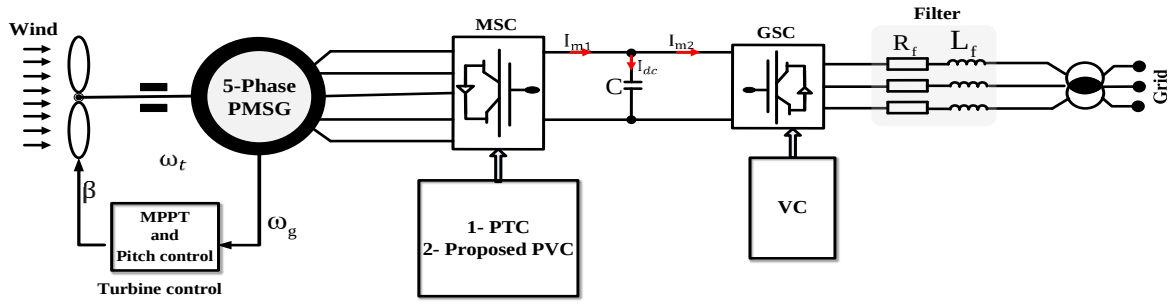

Fig. 6. Illustration of adopted control systems on MSC and GSC converters

3.1. Vector Control (VC) Applied to the GSC

In Fig. 7, the vector control approach for the GSC employs a nested-loop architecture with two current loops, an inner loop and an outer. The active and reactive power equations show that the dq grid current and voltage components are cross-coupled, giving a difficult regulation of active and reactive power, as follows:

$$P_g = 1.5\left[u_{df,(k)}i_{df,(k)} + u_{qf,(k)}i_{qf,(k)}\right] \tag{26}$$

$$Q_g = 1.5\left[u_{qf,(k)}i_{df,(k)} - u_{df,(k)}i_{qf,(k)}\right] \tag{27}$$

These formulas show the ability to control P_g and Q_g by control $i_{df,(k)}$ and $i_{qf,(k)}$. The grid voltage is centered on the q-axis reference, resulting in a d-axis voltage of zero. Using the voltage-oriented control approach, the active and reactive power equations may be expressed as follows.

$$P_g = 1.5\left[u_{qf,(k)}i_{qf,(k)}\right] \tag{28}$$

$$Q_g = 0 \tag{29}$$

In this configuration, the DC-link voltage is controlled by the q-axis loop, and reactive power regulation or grid voltage support is handled by the d-axis loop. The interior current loop's control strategy is formulated using the subsequent equations to generate the reference signal.

$$u^*_{df} = \left[u'_{df} - L_f\omega_{s,(k)}i_{qf,(k)} - u_{df,(k)}\right] \tag{30}$$

$$u^*_{qf} = \left[u'_{qf} - L_f\omega_{s,(k)}i_{df,(k)} + u_{qf,(k)}\right] \tag{31}$$

According to the grid system in Fig. 7, the VOC requires an outer loop (DC voltage loop) to provide a reference direct grid current for active power, referred to as (31) by conveying the errors between measured DC voltage and DC reference to PI control.

An inner current loop is required to manage reactive power and remove current cross-coupling between the d and q components, which requires direct compensation of some terms ($L_f\omega_{s,(k)}i_{df,(k)}$). The Phase Locked Loop (PLL) calculates the grid voltage space vector angle to modify the coordinates. As previously stated, the reference frame's q-axis aligns with the grid voltage space vector. The direct grid voltage therefore equals zero. To get a unity power factor, set the reference of the direct grid current to zero ($i_{df,(k)}$=0). Finally, gate drive pulses are produced using a PWM.

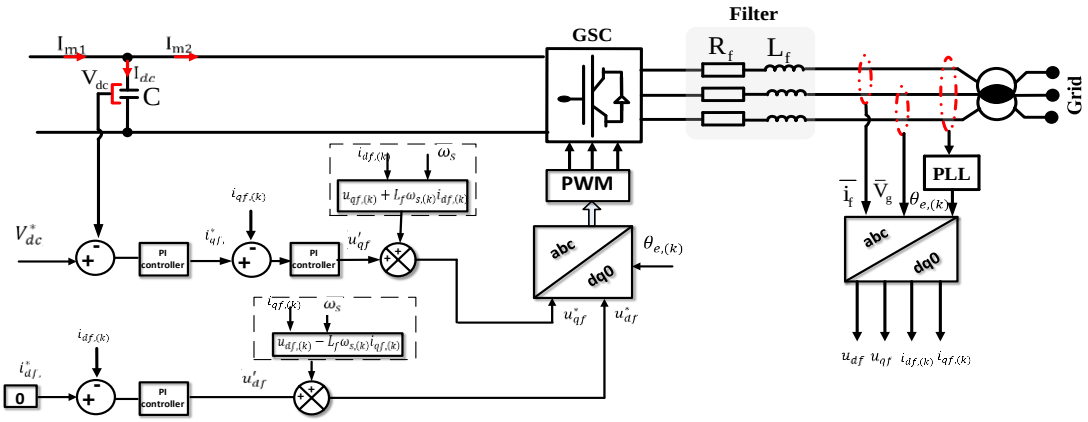

Fig. 7. Voltage-oriented control applied to GSC

3.2. Machine-Side Converter (MSC) Control

This section outlines the techniques applied in the (MSC), whereas the GSC control is VOC. First, the predictive torque control will be covered in Section 3.2.1, then the proposed predictive voltage control approach will be illustrated in Section 3.2.2.

3.2.1. Classical Predictive Torque Control (PTC)

The responsibility of the PTC is to regulate the generator's flux and torque. In order to design the control system, it is necessary to utilize a cost function that regulates the absolute errors of the flux and torque. The cost function employs the weighting factor (ω_f)that equalizes torque and flux due to their inherent differences. In the traditional DTC method, this cost function substitutes for hysteresis controllers and lookup tables. As a result, a cost function of the PTC [58] can be mathematically represented as follows:

$$\nabla^{j}_{(k+1)} = \left|T^{*}_{g,(k+1)} - \tilde{T}_{g,(k+1)}\right|^{j} + \omega_f\left|\varphi^{*}_{g,(k+1)} - \tilde{\varphi}_{g,(k+1)}\right|^{j} \tag{32}$$

Where $T^{*}_{g,(k+1)}$ refers to reference torque which can be obtained from the wind control system, $\tilde{T}_{g,(k+1)}$ is the predicted torque signal, $\tilde{\varphi}_{g,(k+1)}$ is the predicted flux signal, and $\varphi^{*}_{g,(k+1)}$ refers to reference flux. The reference flux ($\varphi^{*}_{g,(k+1)}$) which can be calculated from the reference dqxy components of current as follows:

$$\varphi^{*}_{g,(k+1)} = \sqrt{\left(L_s\overbrace{i^{*}_{ds,(k+1)}}^{0.0} + \varphi_f\right)^2 + \left(L_s i^{*}_{qs,(k+1)}\right)^2 + \left(L_l\overbrace{i^{*}_{xs,(k+1)}}^{0.0}\right)^2 + \left(L_l\overbrace{i^{*}_{ys,(k+1)}}^{0.0}\right)^2} \tag{33}$$

As seen the references of the d component is zero because the permanent magnet can be kept from demagnetizing in interior PMSGs if the d-axis current is consistently kept at zero, also x and y components are set to zero. The reference current $i^{*}_{qs,(k+1)}$ can be evaluated by:

$$i^{*}_{qs,(k+1)} = \frac{T^{*}_{g,(k+1)}}{2.5p\varphi_f} \tag{34}$$

The weighting factor can be obtained as follows:

$$\omega_f = \frac{T_{nominal}}{\varphi_{nominal}} \tag{35}$$

Additionally, the predicted torque signal $\tilde{T}_{g,(k+1)}$ is calculated as:

$$\tilde{T}_{g,(k+1)} = \frac{5}{2} p \tilde{\imath}_{qs,(k+1)}\, \varphi_f \tag{36}$$

The predicted signal $\tilde{\varphi}_{g,(k+1)}$ can be evaluated from:

$$\tilde{\varphi}_{g,(k+1)} = \sqrt{\left(L_s \tilde{\imath}_{ds,(k+1)} + \varphi_f\right)^2 + \left(L_s \tilde{\imath}_{qs,(k+1)}\right)^2 + \left(L_l \tilde{\imath}_{xs,(k+1)}\right)^2 + \left(L_l \tilde{\imath}_{ys,(k+1)}\right)^2} \tag{37}$$

Similar to (27) the predicted stator currents $(\tilde{\imath}_{ds,(k+1)}, \tilde{\imath}_{qs,(k+1)}, \tilde{\imath}_{xs,(k+1)}, \tilde{\imath}_{ys,(k+1)})$ are calculated as follows:

$$\begin{gathered} \tilde{\imath}_{ds,(k+1)} = i_{ds,(k)} + \left(\frac{di_{ds,(k)}}{dt}\right) T_s,\ \tilde{\imath}_{qs,(k+1)} = i_{qs,(k)} + \left(\frac{di_{qs,(k)}}{dt}\right) T_s, \\ \tilde{\imath}_{xs,(k+1)} = i_{xs,(k)} + \left(\frac{di_{xs,(k)}}{dt}\right) T_s,\ \tilde{\imath}_{ys,(k+1)} = i_{ys,(k)} + \left(\frac{di_{ys,(k)}}{dt}\right) T_s \end{gathered} \tag{38}$$

The PTC measures stator voltages and current, samples all variables, and computes prediction values of dq stator current using Equation (38). These values are then used to predict stator flux and torque, as well as the reference. In the last phase, the cost function minimizes errors in the reference and predicted values of the stator and torque according to (32) and applies the voltage to achieve this, by utilizing the eight voltage vectors as it uses the FCS technique to select the vectors. Select the initial vector that keeps the cost function as the lowest possible value and applies it to the converter terminal. An illustration of the PTC scheme for the MSC is shown in Fig. 8. A detailed flow chart of the proposed control system is shown in Fig. 9.

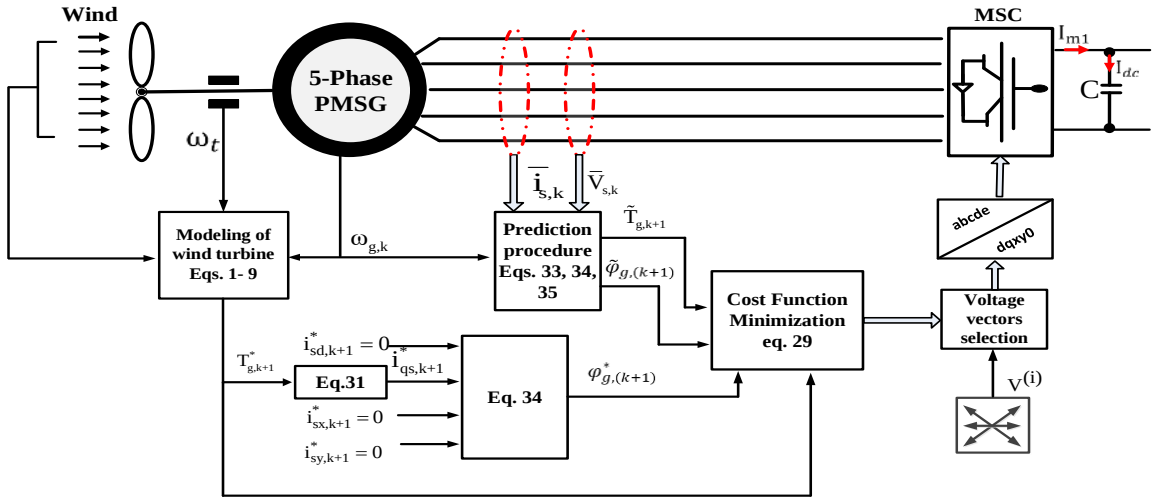

Fig. 8. Predictive torque control scheme applied to MSC

3.2.2. Proposed Predictive Voltage Control (PVC) Method

In order to overcome the drawbacks of the traditional MPC systems discussed previously, an efficient (PVC) approach was developed. The fundamental concept relies upon a reliable cost function devoid of parameter-dependent components. The generator $dqxy$ stator voltage components are chosen as the cost function variables in order to satisfy this stipulation. This cost function does

not necessitate a weighting value because its variables have identical units. The cost function is shown as follows:

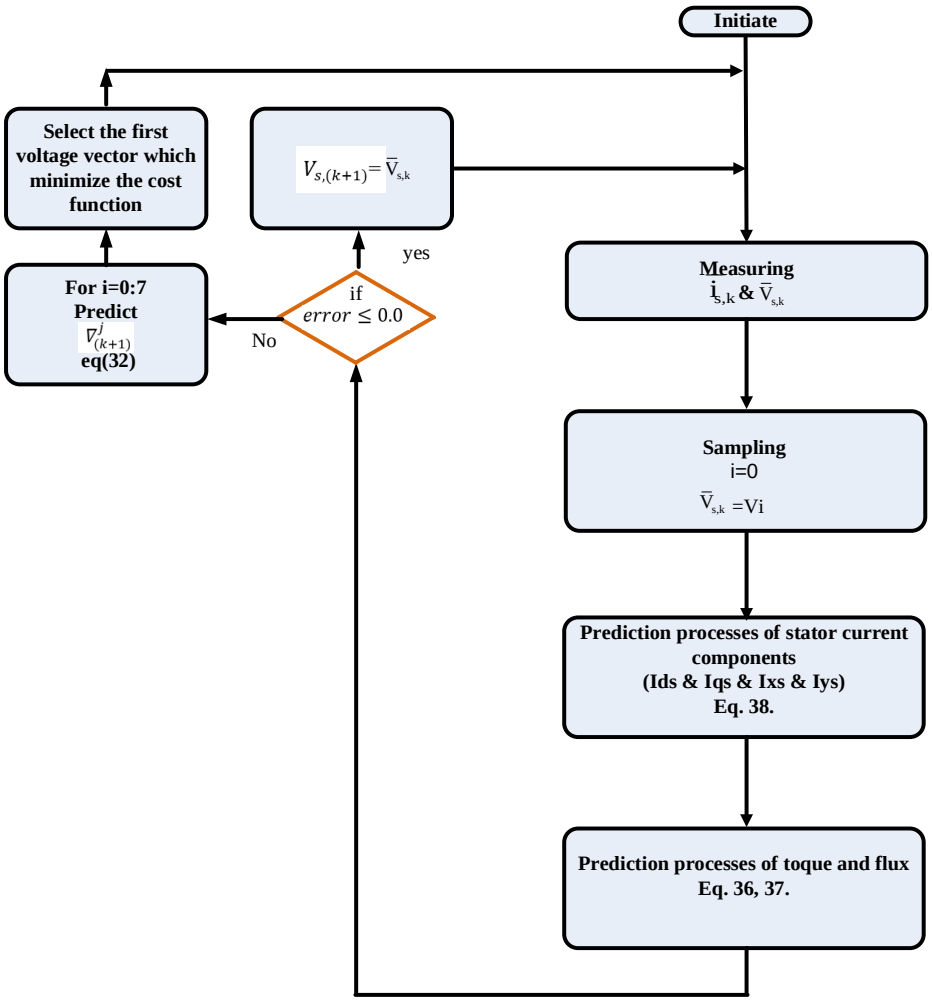

Fig. 9. Detailed flow chart of PTC considering MSC

$$\cap^{j}_{(k+1)}= \left|V^{r}_{ds,(k+1)} - V_{ds,(k+1)}\right|^{j} + \left|V^{r}_{qs,(k+1)} - V_{qs,(k+1)}\right|^{j} + \left|V^{r}_{xs,(k+1)} - V_{xs,(k+1)}\right|^{j} + \left|V^{r}_{ys,(k+1)} - V_{ys,(k+1)}\right|^{j} \quad (39)$$

Where $(V_{ds,(k+1)},\ V_{qs,(k+1)}, V_{xs,(k+1)}, V_{ys,(k+1)})$ are actual voltage components which directly derived from the converter's switching states using the FCS principle, which allows for the selection of a finite number of voltage vectors. Furthermore, $(V^{r}_{ds,(k+1)},\ V^{r}_{qs,(k+1)},\ V^{r}_{xs,(k+1)}\ V^{r}_{ys,(k+1)})$ are the reference voltage signals that are generated via employing the backstepping theory as follows. The current error signal can be represented as:

$$\epsilon_{ds,(k+1)}= i^{r}_{ds,(k+1)} - i_{ds,(k+1)}\ \ \epsilon_{qs,(k+1)}= i^{r}_{qs,(k+1)} - i_{qs,(k+1)}$$
$$\epsilon_{xs,k+1}= i^{r}_{xs,(k+1)} - i_{xs,(k+1)}\ \text{ and } \epsilon_{ys,k+1}= i^{r}_{ys,(k+1)} - i_{ys,(k+1)} \quad (40)$$

The current error derivative can be written using the current derivative in (10:13) as follows:

$$\dot{\epsilon}_{ds,(k+1)}= \frac{-1}{L_s}\left[-R_s i_{ds,(k+1)} + pL_s\omega_{g,(k+1)} i_{qs,(k+1)} + V_{ds,(k+1)}\right] \quad (41)$$

$$\dot{\epsilon}_{qs,(k+1)}=\frac{di^{r}_{qs,(k+1)}}{dt}-\frac{1}{L_s}-R_s i_{qs,(k+1)} \\ -pL_s\omega_{g,(k+1)}i_{ds,(k+1)}-p\omega_{g,(k+1)}\varphi_f+V_{qs,(k+1)} \tag{42}$$

$$\dot{\epsilon}_{xs,(k+1)}=\frac{-1}{L_l}\left[-R_s i_{xs,(k+1)}+V_{xs,(k+1)}\right] \tag{43}$$

$$\dot{\epsilon}_{ys,(k+1)}=\frac{-1}{L_l}\left[-R_s i_{ys,(k+1)}+V_{ys,(k+1)}\right] \tag{44}$$

Then the speed error can be expressed as

$$\epsilon_{\omega,(k+1)}=\omega^{r}_{g,(k+1)}-\omega_{g,(k+1)} \tag{45}$$

Where $\omega^{r}_{g,(k+1)}$ is the desired speed given by (6) the speed error dynamics' derivative utilizing (7) can be defined by:

$$\dot{\epsilon}_{\omega,(k+1)}=\frac{d\omega^{r}_{g,(k+1)}}{dt}-\frac{d\omega_{g,(k+1)}}{dt}=\frac{-1}{J_g}\left[T_{t,(k+1)}-\frac{5}{2}\varphi_f i_{qs,(k+1)}-D\omega_{g,(k+1)}\right] \tag{46}$$

To ensure the stability of the dynamic system, the function of Lyapunov's is implemented as [71]:

$$\ell_{1,(k+1)}=\frac{1}{2}\dot{\epsilon}^{2}{}_{\omega,(k+1)} \tag{47}$$

By differentiating (47) and using (46), the equation will be:

$$\dot{\ell}_{1,k+1}=\epsilon_{\omega,(k+1)}\dot{\epsilon}_{\omega,(k+1)}=-k_\omega\ \epsilon^{2}{}_{\omega,(k+1)} \\ +\frac{\epsilon_{\omega,(k+1)}}{J_g}\left[-T_{t,(k+1)}+\frac{5}{2}p\varphi_f i_{qs,(k+1)}+T_{f,(k+1)}+k_\omega J_g\ \epsilon_{\omega,(k+1)}\right] \tag{48}$$

where k_ω is a positive constant.

To attain convergence and guarantee zero tracking error, it is necessary for the value of (48) to be negative. As a result, the currents $i_{ds,(k+1)}$ and $i_{qs,(k+1)}$ are regarded as artificial system inputs. The expression for the synthetic input reference current $i^{r}_{qs,(k+1)}$ can be expressed by:

$$i^{r}_{qs,(k+1)}=\frac{1}{2.5p\psi_{f,k+1}}\left[T_{t,(k+1)}-T_{f,(k+1)}-k_\omega J_g\ \epsilon_{\omega,(k+1)}\right] \tag{49}$$

Thus, the Lyapunov's function derivative of (48) reveals it to be as follows:

$$\dot{\ell}_{1,k+1}=\epsilon_{\omega,(k+1)}\dot{\epsilon}_{\omega,(k+1)}=-k_\omega\ \epsilon^{2}_{\omega,(k+1)}<0 \tag{50}$$

As can be observed, the value of (48) is negative, indicating that the dynamic basis created in (49) satisfies the tracking stability criteria. In accordance with the aforementioned hypothesis, the error dynamic in (42) can be mathematically represented by:

$$\dot{\epsilon}_{qs,(k+1)}=\frac{\left[D-k_\omega J_g\right]}{2.5p\varphi_f}\dot{\epsilon}_{\omega,(k+1)} \\ +\frac{1}{L_s}\left[R_s i_{qs,(k+1)}+pL_s\omega_{g,(k+1)}i_{ds,(k+1)}+p\omega_{g,(k+1)}\varphi_f-V_{qs,(k+1)}\right] \tag{51}$$

The derivative dynamics of speed error $\dot{\epsilon}_{\omega,(k+1)}$ may be reconstructed from (46) assuming (40) and (49) as

$$\dot{\epsilon}_{\omega,(k+1)}=\frac{1}{J_g}\left[-k_\omega J_g\ \epsilon_{\omega,(k+1)}-\frac{5}{2}p\varphi_f\ \epsilon_{qs,(k+1)}\right] \tag{52}$$

Then by substituting from (52) into (51), the result is as follows:

$$\begin{aligned}\dot{\epsilon}_{qs,(k+1)}=&\frac{[D-k_\omega J_g]}{2.5pJ_g\varphi_f}\left[-k_\omega J_g\ \epsilon_{\omega,(k+1)}-\frac{5}{2}p\varphi_f\ \epsilon_{qs,(k+1)}\right]\\&+\frac{1}{L_s}\left[R_s i_{qs,(k+1)}+pL_s\omega_{g,(k+1)}i_{ds,(k+1)}+p\omega_{g,(k+1)}\varphi_f-V_{qs,(k+1)}\right]\end{aligned} \tag{53}$$

The system is then suggested to be controlled by a new Lyapunov algorithm that makes use of the voltage vectors in the following way.

$$\ell_{2,(k+1)}=\frac{1}{2}\epsilon^2_{\omega,(k+1)}+\frac{1}{2}\epsilon^2_{ds,(k+1)}+\frac{1}{2}\epsilon^2_{qs,(k+1)}+\frac{1}{2}\epsilon^2_{xs,(k+1)}+\frac{1}{2}\epsilon^2_{ys,(k+1)} \tag{54}$$

Taking the time derivative of the previous equation

$$\begin{aligned}\dot{\ell}_{2,(k+1)}=&\epsilon_{\omega,(k+1)}\dot{\epsilon}_{\omega,(k+1)}+\epsilon_{ds,(k+1)}\dot{\epsilon}_{ds,(k+1)}\\&+\epsilon_{qs,(k+1)}\dot{\epsilon}_{qs,(k+1)}+\epsilon_{xs,(k+1)}\dot{\epsilon}_{xs,(k+1)}+\epsilon_{ys,(k+1)}\dot{\epsilon}_{ys,(k+1)}\end{aligned} \tag{55}$$

By using (41)-(44) and (48), the Lyapunov derivative is expressed as follows:

$$\begin{aligned}\dot{\ell}_{2,(k+1)}=&-k_{id}\ \epsilon^2_{ds,(k+1)}-k_{iq}\ \epsilon^2_{qs,(k+1)}-k_{ix}\ \epsilon^2_{xs,(k+1)}-k_{iy}\ \epsilon^2_{ys,(k+1)}-k_\omega\ \epsilon^2_{\omega,(k+1)}\\&+\frac{\epsilon_{qs,(k+1)}}{L_s}\left[\frac{L_s[D-k_\omega J_g]}{2.5pJ_g\varphi_f}\left(-k_\omega J_g\ \epsilon_{\omega,(k+1)}-\frac{5}{2}p\varphi_f\ \epsilon_{qs,``k+1)}\right)+R_s i_{qs,(k+1)}\right.\\&\quad+pL_s\omega_{g,(k+1)}i_{ds,(k+1)}+p\omega_{g,(k+1)}\varphi_f-V_{qs,(k+1)}+k_{iq}L_s\ \epsilon_{qs,(k+1)}\\&\quad\left.-\frac{2.5p\varphi_f L_s}{J_g}\epsilon_{\omega,(k+1)}\right]\\&+\frac{\epsilon_{ds,(k+1)}}{L_s}\left[R_s i_{ds,(k+1)}-pL_s\omega_{g,(k+1)}i_{qs,(k+1)}\right.\\&\quad\left.-V_{ds,(k+1)}+k_{id}L_s\ \epsilon_{ds,(k+1)}\right]\\&+\frac{\epsilon_{xs,(k+1)}}{L_l}\left[R_s i_{xs,(k+1)}-V_{xs,(k+1)}+k_{ix}L_l\ \epsilon_{xs,(k+1)}\right]\\&+\frac{\epsilon_{ys,(k+1)}}{L_l}\left[R_s i_{ys,(k+1)}-V_{ys,(k+1)}+k_{iy}L_l\ \epsilon_{ys,(k+1)}\right]\end{aligned} \tag{56}$$

where k_{id}, k_{iq}, k_{ix} and k_{iy} are positive constants.

To guarantee the stability of the system, the derivative $\dot{\ell}_{2,(k+1)}$ in (48) To ensure zero error, the derivative should have a negative value. Accordingly, reference voltages that fulfill this criterion and are to be used in the designed predictive controller's cost function in (39) are described as follows:

$$V^r_{ds,(k+1)}=R_s i_{ds,(k+1)}-pL_s\omega_{g,(k+1)}i_{qs,(k+1)}+k_{id}L_s\ \epsilon_{ds,(k+1)} \tag{57}$$

$$\begin{aligned}V^r_{qs,(k+1)}=&\frac{L_s[D-k_\omega J_g]}{2.5pJ_g\varphi_f}\left(-k_\omega J_g\ \epsilon_{\omega,(k+1)}-\frac{5}{2}p\varphi_f\ \epsilon_{qs,(k+1)}\right)\\&+R_s i_{qs,(k+1)}+pL_s\omega_{g,(k+1)}i_{ds,(k+1)}+p\omega_{g,(k+1)}\varphi_f\end{aligned} \tag{58}$$

$$+ k_{iq}L_s \in_{qs,(k+1)} - \frac{2.5p\varphi_f L_s}{J_g} \in_{\omega,(k+1)}$$

$$V^r_{xs,(k+1)} = R_s i_{xs,(k+1)} + k_{ix}L_l \in_{xs,(k+1)} \quad (59)$$

$$V^r_{ys,(k+1)} = R_s i_{ys,(k+1)} + k_{iy}L_l \in_{ys,(k+1)} \quad (60)$$

Once the voltages used as references have been assessed, the cost function implemented in (39) can be estimated. This enables the control to determine the most appropriate vector to handle at each instant the nominal error remains constant at zero.

The proposed controller's system design is shown in Fig. 10. The operation begins by tracking the five-phase voltage and current signals, after which the system carries out coordinate transformation and predicts current values. Following that, the backstepping algorithm uses these values of reference and predicted currents to construct the reference voltage, which are then utilized to assess the cost function of (39). The control then calculates the cost function's value at every instant in time, checks and selects the first voltage vector that minimizes the function, and applies it to the five-phase converter. A detailed flow chart of the proposed control system is shown in Fig. 11.

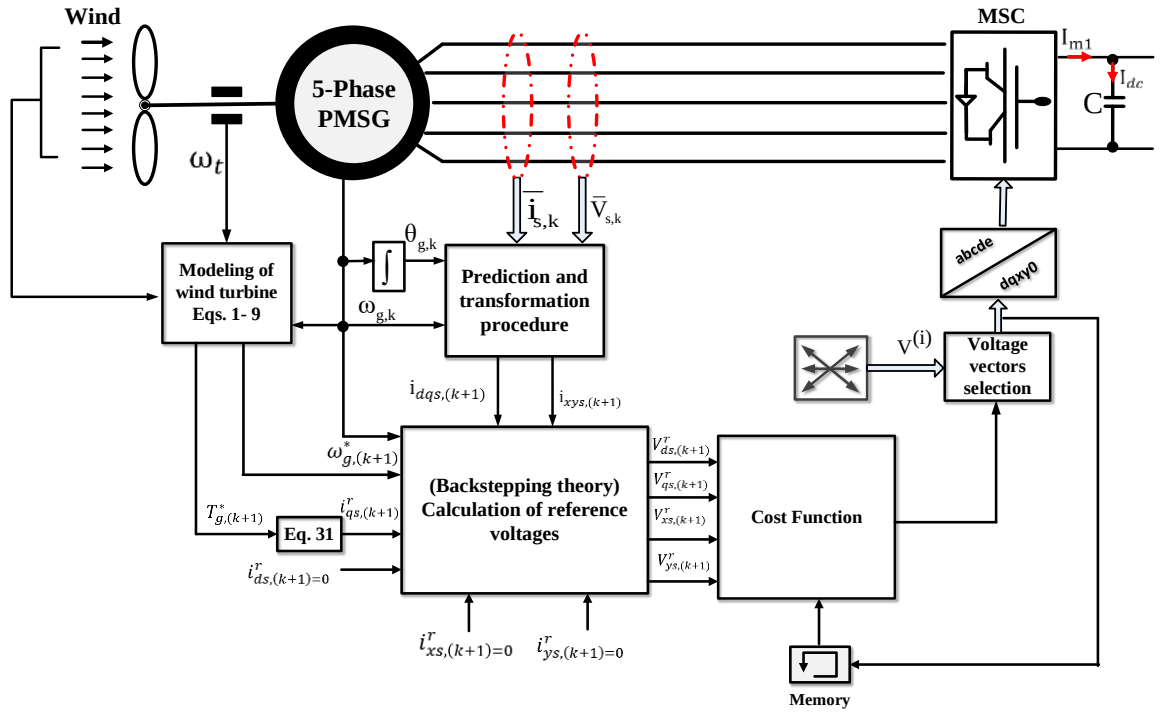

Fig. 10. The formulated PVC scheme for MSC

4. Performance Evaluation Results

This analysis is performed upon vector control (VC) at the grid side converter to oversee operations and guarantee unity pf operation. while the control techniques of the five-phase PMSG are two predictive controllers (PTC, proposed PVC). The wind speed variation curve (V_w) is in Fig. 12, whereas Fig. 13 shows the generator shaft speed (ω_g) under the two predictive control approaches and it's obvious that the shaft speed is varying considering wind speed variation due to the control algorithms in wind turbines. Fig. 14 depicts the turbine coefficient (C_p), which varies as wind speed exceeds the designated threshold, hence validating MPPT and PAC. Fig. 15 and Fig. 16 show that the blade angle (β) increases when the wind surpasses its specified value, yet the tip ratio (λ) remains appropriate for MPPT.

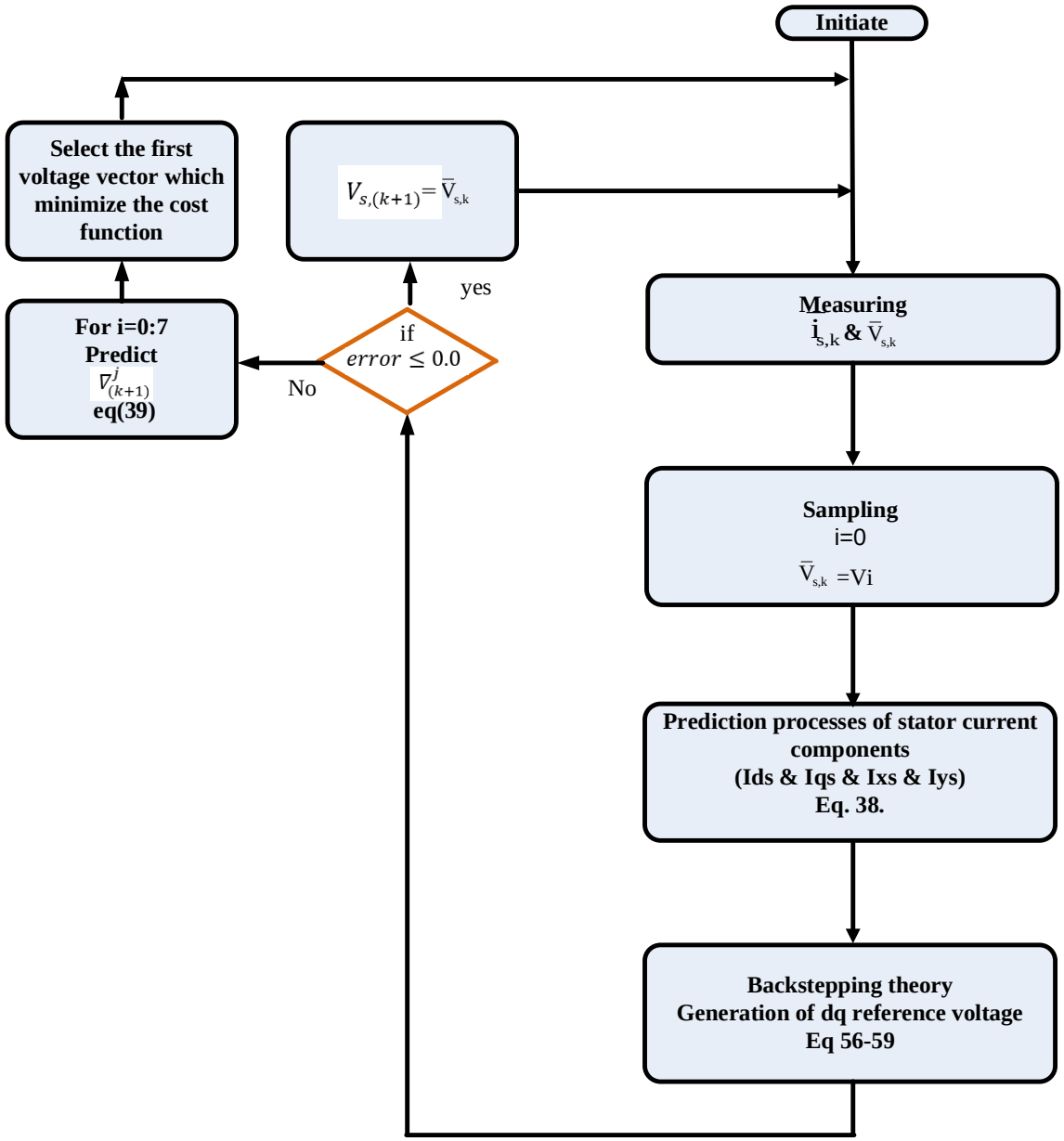

Fig. 11. A detailed flow chart of proposed PVC considering MSC

The vector control (VC) results at the grid side converter (GSC) are considered when analyzing the generator dynamics with two predictive controllers including the proposed model. Introducing the suggested PVC control, which, when compared to alternative predictive algorithms, has the fastest dynamic reaction and the best smooth variation. To demonstrate the controller performance. Fig. 17 depicts the generator's active power, demonstrating that the proposed control model offers reduced power volatility than the standard PTC which improves the caliber of power that is being supplied, which attests to the fact that the proposed PVC has the quickest dynamic response and fewest ripples when compared to the other predictive control methods. This is because the voltage signal is controlled by the const function, which takes control of the voltage signal directly from the controller's output to the machine winding, whereas the cost function requires estimating torque and flux as in PTC. As a result, any changes to the machine's specification parameters won't affect the control. consequence, PVC ripple is reduced as well as commutation burden and resilience.

That is also guaranteed by the torque depicted in Fig. 18 which starts to change in response to changes in wind speed. Of all the predictive controllers, the suggested PVC algorithm has the lowest

ripple fluctuation and the greatest dynamic response. This is known as supplying the voltage to the machine straight from the controller's output, without any kind of estimation or prediction like in PTC. As a result, any errors or changes to the machine's parameters have no effect on the control, which reduces computation, burden, and ripple in the PVC and increases its robustness. The weighting element was removed from the cost function of the proposed PVC, but not the PTC, which is another explanation for the low ripple and reduced computing capacity. In contrast to other predictive controllers, PVC has the fastest dynamic response because the voltage is the first variable to interact with the windings. Fig. 19 displays a comparison between the PTC and the proposed approach with the reference value of dq generated current. The dq generated current changes according to the wind speed. Aside from that, the d-axis component stays constant and follows the reference value ($i^*_{ds,(k+1)}$ = 0), but the q-axis current fluctuates in response to variations in power and mechanical torque as well as wind speed fluctuation. As a result, the form of the current is comparable to the shapes of the torque and power.

The proposed controller reduces ripples in the currents as compared to the PTC methods. Fig. 20 depicts the DC bus voltage fluctuations under the two controllers, demonstrating that the proposed controller delivers significantly reduced voltage swings around its reference level and the fastest dynamic response. Fig. 21 depicts power signals at the GSC, demonstrating that a proper unity of pf is attained because the d-axis grid current is held at zero tracking the reactive power, and the change in active power is tracked by q-axis grid current. Meanwhile, the outcomes show less turbulence when the predictive controller is constructed. Fig 24 and Fig. 25 show the generated currents when operating under the two predictive controllers.

The developed controller produces consistently distributed sinusoidal currents with significantly fewer ripples. As well as the proposed PVC. These results illustrate that the proposed PVC method has the lowest current harmonics. This means that when voltage is applied without considering machine parameters, the voltage oscillation is reduced. As we obtain the current from the voltage, the harmonic distortion of the current decreases. The total harmonic distortion THD is a metric used to evaluate the level of distortion in a waveform compared to its fundamental frequency. It is calculated as the ratio of the sum of the powers of all harmonic components to the power of the fundamental frequency. FFT analysis was also employed to investigate the currents generated by the stator. This fact is verified mathematically in Table 1 and approved graphically in Fig. 22, and Fig. 23 which depict the (THD) analysis of the generated current under the two predictive controllers.

The designed predictive control can be applied to other generator types, such as double-field induction generators, other multiphase generators, or turbine wind generators, the strategy enhancement of control techniques is to achieve superior performance and efficiency. The implementation of non-linear control techniques for wind-driven five-phase PMSGs poses difficulties and possibilities in terms of scalability, flexibility, and system performance. Research highlights the necessity for complex mathematical models and innovative control techniques like Integral Sliding Mode Control (ISMC) with Space Vector Pulse Width Modulation (SVPWM) to boost system efficiency and power quality. Research indicates that it is beneficial to investigate advanced control techniques such as combine intelligent fuzzy logic systems with robust fractional order sliding mode control and applying sliding mode pulse-width modulation for current-controlled five-leg converters in wind energy systems. Furthermore, exploring the potential of enhancing the design and properties of five-phase PMSGs through the utilization of Improved Magnetic Circuit (IMC) models in the context of wind power applications holds great promise for future study. The future research on wind-driven five-phase PMSGs intends to develop renewable energy technologies for sustainable power production by improving control algorithms, increasing system efficiency, and optimizing generator design.

The developed controller produces consistently distributed sinusoidal currents with significantly fewer ripples. This fact is verified mathematically in Table 2 which depicts the THD examination of the current under the two predictive controllers, also the computation time for predictive control

algorithms is a significant issue, as it is well-established that model predictive controllers are time-consuming.

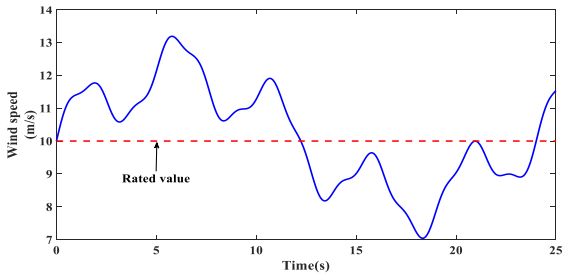

Fig. 12. Wind speed variation

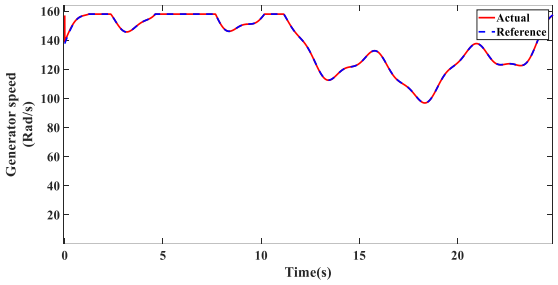

Fig. 13. Generator shaft speed

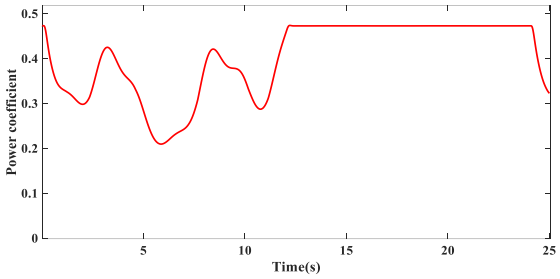

Fig. 14. Power coefficient

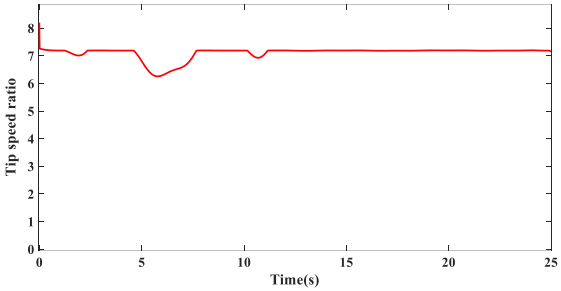

Fig. 15. Tip speed ratio

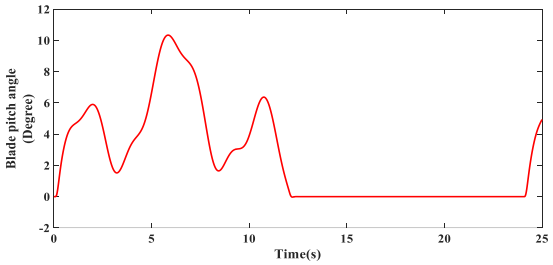

Fig. 16. Blade pitch angle

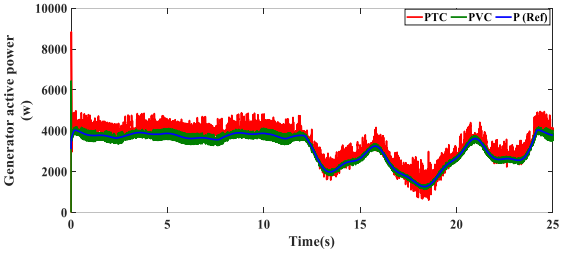

Fig. 17. Generated active power

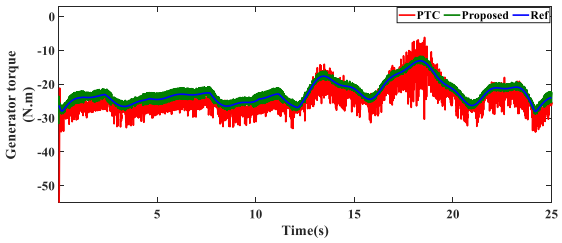

Fig. 18. Generator torque

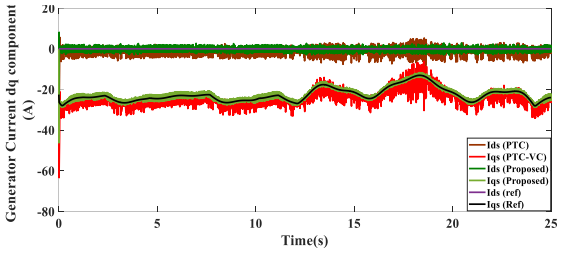

Fig. 19. Generator current d-q components (A)

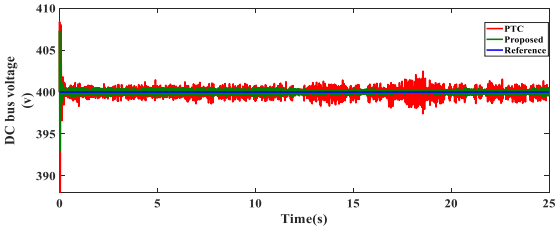

Fig. 20. DC bus voltage

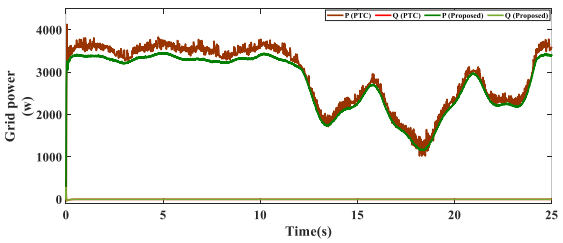

Fig. 21. Grid active and reactive powers

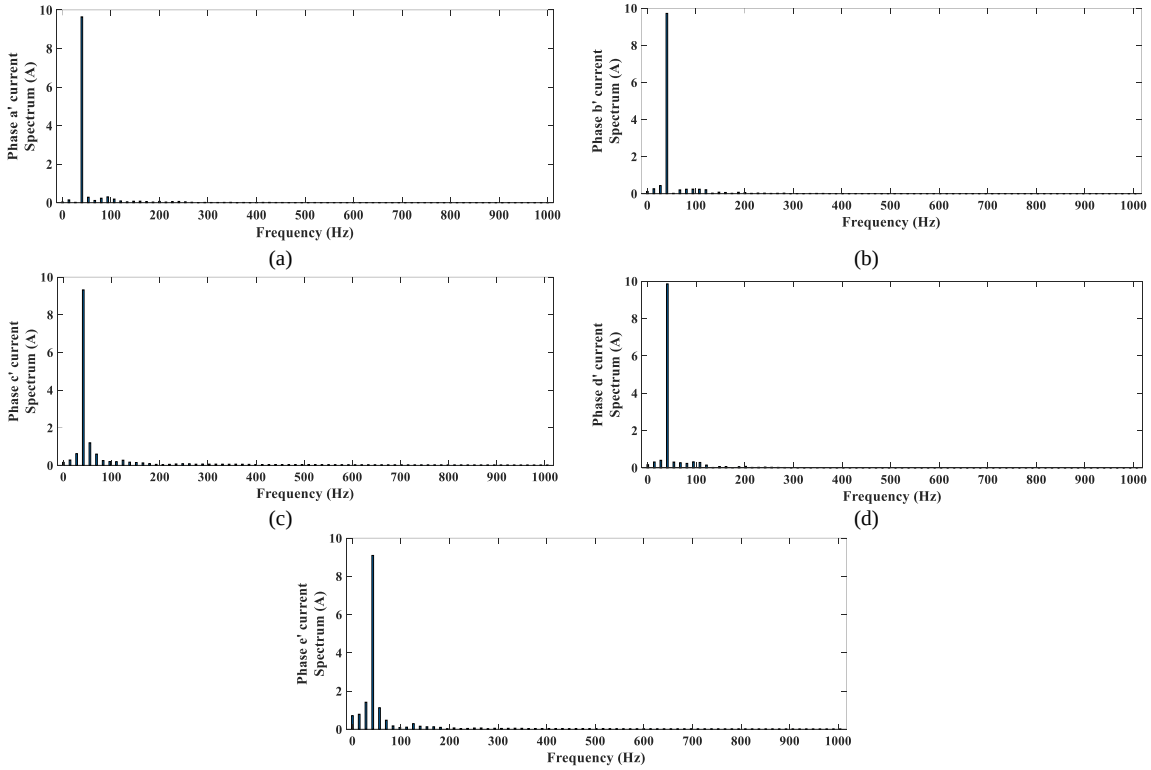

Fig. 22. Currents THD spectrums under classic PTC

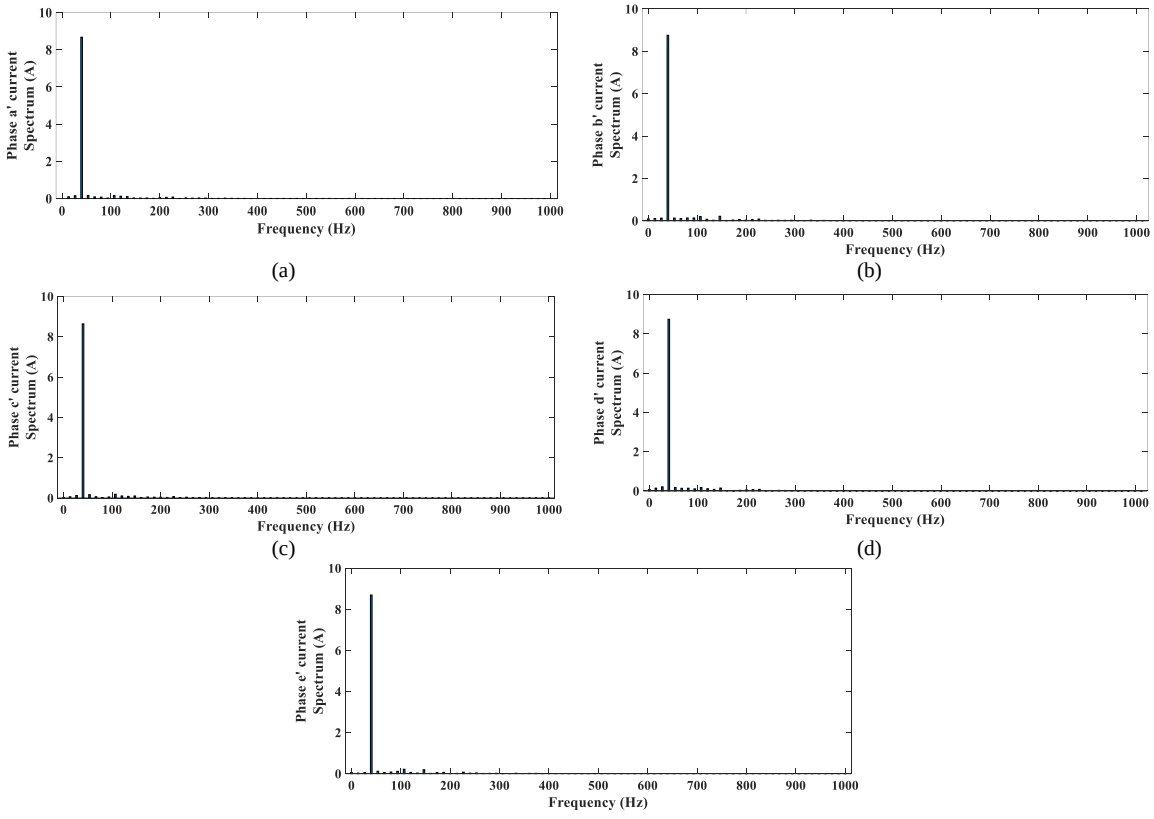

Fig. 23. Currents THD spectrums under the proposed PVC

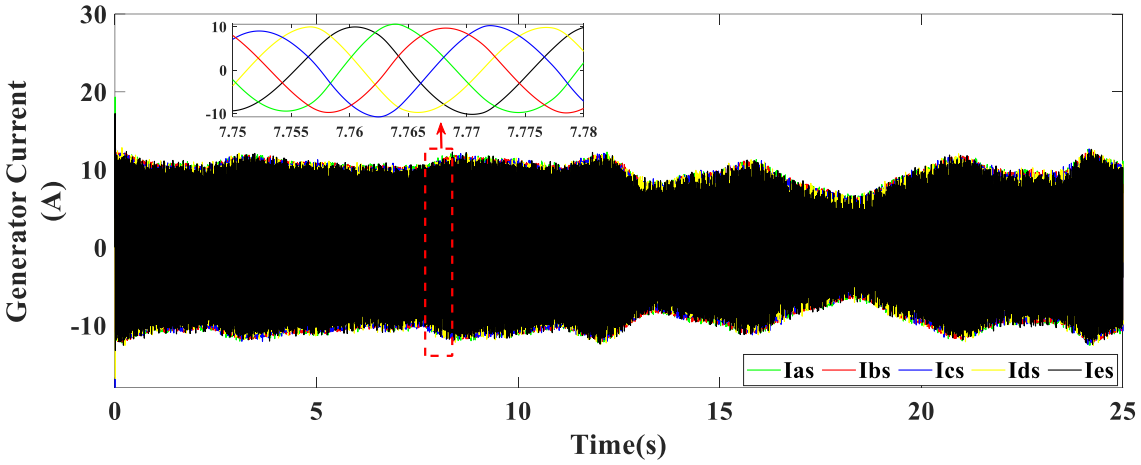

Fig. 24. Generator currents considering classic PTC

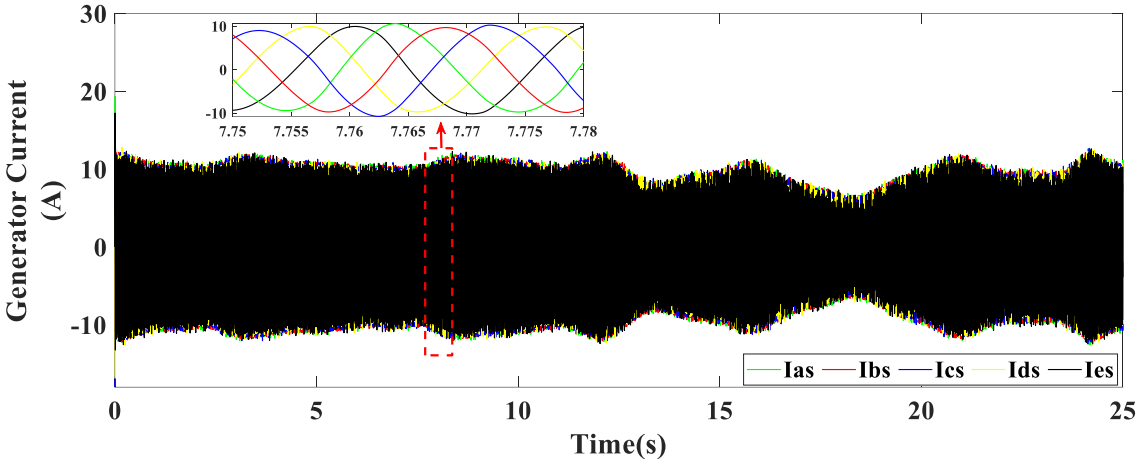

Fig. 25. Generator currents considering the proposed PVC controller

Consequently, a comparison was also conducted between the two predictive controllers (PTC, and devised PVC) in terms of the number of commutations performed during the code execution as shown in Table 3. Also, the ripple content of the two predictive controllers' is compared in Table 4 in two different of time, demonstrating that the PVC technique has a lower ripple content than the MPCC approach. The data support the results.

Table 2. THD analysis for VC at GSC

Phase	PTC Ref [72]	Proposed PVC
'a'	Fundamental (9.64039 A) THD (2.33 %)	Fundamental (8.66809A) THD (1.46%)
'b'	Fundamental (9.71911 A) THD (2.78 %)	Fundamental (8.75611 A) THD (1.43%)
'c'	Fundamental (9.31899 A) THD (3.94 %)	Fundamental (8.63686A) THD (1.09 %)
'd'	Fundamental (9.85665 A) THD (2.48 %)	Fundamental (8.73834 A) THD (1.76%)
'e'	Fundamental (9.09155 A) THD (3.72 %)	Fundamental (8.69109 A) THD (0.99%)

Table 3. Comparison in terms of performed commutations by the predictive controllers

Technique	Number of commutations	Switching frequencies
PTC	1.45e+4	2.41 KHz
Proposed PVC	1.04e+4	1.73 KHz

Table 4. The ripple content of the actual values deviates from their reference values

Technique	Ripples of Active Power (Watt)		Ripples Developed Torque (N.m)		Ripples of d-Current Component (A)		Ripples of q-Current component (A)	
	Case 1	Case 2	Case 1	Case 2	Case 1	Case 2	Case 1	Case 2
PTC	349.7	495.085	2.69	4.016	2.89	4.488	2.35	4.05
Proposed PVC	100.8	123.22	0.915	1.085	0.745	1.04	1.515	0.95

5. Conclusion

Improving the dynamics of a renewable energy system is the focus of the presented research. The system operates in two distinct controllers during the machine connection (PTC, proposed PVC) whereas the GSC control is VC. A comprehensive exposition of every system unit is furnished. The system consists of a rectifier, DC bus, and converter arrangement that integrates a wind-driven generator into the grid. To optimize the power output of the wind turbine, the MPPT technique is employed. The newly developed predictive controller additionally improves the dynamics of the five-phase generator. The results acquired demonstrate and validate the superior performance of the newly developed predictive approach in comparison to the traditional control method for the wind generation system. By guarantees the fastest dynamic response, lowest ripple, lowest computation capacity, independence of machine parameters, less variation in the variables under control, and reduced current harmonics as the THD of traditional PTC is 3.05%. It's a large value as compared to the proposed PVC, as the THD is reduced to 1.346%. Also, the developed controller produces consistently distributed sinusoidal currents with significantly fewer ripples. This fact is verified mathematically as the ripples decreased from 24.25% of the traditional PTC to 10.886% of the proposed PVC. This has been certified and enhanced the quality of the electricity that is produced when depending on the proposed PVC. The results demonstrate that the proposed PVC controller exhibited exceptional dynamic performance and minimal computational demands, as evidenced by its straightforward design, minimal oscillations, and low current harmonics. Consequently, it affects the efficiency of the generated active power, leading to enhanced system efficiency by minimizing fluctuations. This, in turn, leads to improved power injected into the grid and reduced switching losses on the GSC and the MSC, thereby enhancing the efficiency of power converters and ensuring a prolongation of the lifespan of the switches. Moreover, it provides robustness against parameter variations, and external disturbances, which ensures system reliability. Overall, the designed predictive control can be applied to other generator types, such as double-field induction generators, other multiphase generators, or turbine wind generators, after considering their unique structures, as well as the system, can be integrated with other renewable energy sources such as PV systems or different wind turbine environmental conditions. The wind-driven generators can be further controlled via machine learning to improve efficiency and performance such as enhanced methods like FSMC and FBSC.

Author Contribution: All authors contributed equally to the main contributor to this paper. All authors read and approved the final paper.

Funding: This research received no external funding

Conflicts of Interest: The authors declare no conflict of interest.

Abbreviations and Acronyms

PMSG	Permanent magnet synchronous generator	K	Gear ratio
SCIG	Squirrel-cage induction generator	GSC	Grid-side converter
DFIG	Doubly fed induction generator	PAC	Pitch angle control

WECS	Wind energy conversion system	β	Pitch angle
FOC	Field-oriented control	λ	Tip ratio
DTC	Direct torque control	R	Blade radius
SMC	Sliding mode control	ρ	Air density
MPC	Model predictive control	C_p	Power coefficient
MPPT	Maximum power point tracking	J_t and J_g	Turbine and generator inertias
MSC	Machine-side converter	D	Friction constant
R_s	Stator resistance.	L_s	Inductance of the Stator
L_s	Stator inductance	VOC	Voltage-oriented control
PVC	Predictive voltage control	VC	Vector control
PC	Predictive control	p	Pair of poles
PTC	Predictive torque control	ω_g	Mechanical shaft speed
FCS	Finite control set	φ_f	Permanent magnet flux
PWM	Pulse width modulation	R_f	Filter resistance
ω_f	weighting factor	L_f	Filter inductance

References

[1] S. Mathur, H. Waswani, D. Singh, and R. Ranjan, "Alternative fuels for agriculture sustainability: Carbon footprint and economic feasibility," *AgriEngineering*, vol. 4, no. 4, pp. 993-1015, 2022, https://doi.org/10.3390/agriengineering4040063.

[2] F. J. Medaiyese *et al*., "Energy Transition with Dimethyl Ether (An Alternative Fuel to Diesel) to minimise the Environmental Impact," *84th EAGE Annual Conference & Exhibition*, 2023, https://clok.uclan.ac.uk/47006/9/Revised%20paper%20number%20330.pdf.

[3] J. Wolf *et al*., "9.04 - Environmental Issues for Offshore Renewable Energy," *Comprehensive Renewable Energy (Second Edition)*, vol. 9, pp. 25-59, 2022, https://doi.org/10.1016/B978-0-12-819727-1.00036-4.

[4] M. Nurunnabi, N. K. Roy, E. Hossain and H. R. Pota, "Size Optimization and Sensitivity Analysis of Hybrid Wind/PV Micro-Grids- A Case Study for Bangladesh," *IEEE Access*, vol. 7, pp. 150120-150140, 2019, https://doi.org/10.1109/ACCESS.2019.2945937.

[5] X. Xie, Y. Zhang, K. Meng, Z. Y. Dong and J. Liu, "Emergency control strategy for power systems with renewables considering a utility-scale energy storage transient," *CSEE Journal of Power and Energy Systems*, vol. 7, no. 5, pp. 986-995, 2021, https://doi.org/10.17775/CSEEJPES.2019.02320.

[6] P. Sadorsky, "Wind energy for sustainable development: Driving factors and future outlook," *Journal of Cleaner Production*, vol. 289, p. 125779, 2021, https://doi.org/10.1016/j.jclepro.2020.125779.

[7] S. Pira, "The Importance of Renewable Energies with Emphasize on Wind Power," *International Journal of Engineering Research & Technology*, vol. 9, no. 6, pp. 812-822, 2020, https://www.ijert.org/the-importance-of-renewable-energies-with-emphasize-on-wind-power.

[8] A. Eicke, L. Eicke, and M. Hafner, "Wind Power Generation," *The Palgrave Handbook of International Energy Economics*, pp. 171-182, 2022, https://doi.org/10.1007/978-3-030-86884-0_10.

[9] A. I. Beksultanova, P. M. Dzhankhotova, and S. K. Shardan, "Renewable and alternative energy sources. Green energy," *IOP Conference Series: Earth and Environmental Science*, vol. 1045, no. 1, p. 012134, 2022, https://doi.org/10.1088/1755-1315/1045/1/012134.

[10] S. Kumar and K. Rathore, "Renewable energy for sustainable development goal of clean and affordable energy," *International Journal of Materials Manufacturing and Sustainable Technologies*, vol. 2, no. 1, pp. 1-15, 2023, https://typeset.io/pdf/renewable-energy-for-sustainable-development-goal-of-clean-2xwmb24p.pdf.

[11] W. Yang and J. Yang, "Advantage of variable-speed pumped storage plants for mitigating wind power variations: Integrated modelling and performance assessment," *Applied Energy*, vol. 237, pp. 720-732, 2019, https://doi.org/10.1016/j.apenergy.2018.12.090.

[12] O. J. Tola, E. A. Umoh, E. A. Yahaya, O. E. Osinowo, "Permanent magnet synchronous generator connected to a grid via a high speed sliding mode control," *International Journal of Robotics and Control Systems*, vol. 2, no. 2, pp. 379-395, 2022, https://doi.org/10.31763/ijrcs.v2i2.701.

[13] O. Apata and D. T. O. Oyedokun, "Impact Of Statcom On Voltage Stability Of Fixed Speed Wind Farms," *2020 IEEE PES/IAS PowerAfrica*, pp. 1-5, 2020, https://doi.org/10.1109/PowerAfrica49420.2020.9219989.

[14] H. T, C. G and S. D, "SCIG Based Wind Energy Conversion System Fed DC Micro Grid Using DTC," *2023 International Conference on Recent Trends in Electronics and Communication (ICRTEC)*, pp. 1-5, 2023, https://doi.org/10.1109/ICRTEC56977.2023.10111866.

[15] K. Teng, Z. Lu, J. Long, Y. Wang and A. P. Roskilly, "Voltage Build-Up Analysis of Self-Excited Induction Generator With Multi-Timescale Reduced-Order Model," *IEEE Access*, vol. 7, pp. 48003-48012, 2019, https://doi.org/10.1109/ACCESS.2019.2902977.

[16] M. A. Mossa, A. Saad Al-Sumaiti, T. Duc Do and A. A. Zaki Diab, "Cost-Effective Predictive Flux Control for a Sensorless Doubly Fed Induction Generator," *IEEE Access*, vol. 7, pp. 172606-172627, 2019, https://doi.org/10.1109/ACCESS.2019.2951361.

[17] H. Singh and M. Singh, "Investigations On The Control Strategy of Rotor Side Converter In Doubly Fed Induction Generator," *2021 International Conference on Communication, Control and Information Sciences (ICCISc)*, pp. 1-6, 2021, https://doi.org/10.1109/ICCISc52257.2021.9484874.

[18] K. Tamvada and S. Umashankar, "Fuzzy rotor side converter control of doubly Fed induction generator," *Artificial Intelligence and Evolutionary Computations in Engineering Systems*, pp. 657-663, 2018, https://doi.org/10.1007/978-981-10-7868-2_62.

[19] M. A. Mossa, T. Duc Do, A. Saad Al-Sumaiti, N. V. Quynh and A. A. Z. Diab, "Effective Model Predictive Voltage Control for a Sensorless Doubly Fed Induction Generator," *IEEE Canadian Journal of Electrical and Computer Engineering*, vol. 44, no. 1, pp. 50-64, 2021, https://doi.org/10.1109/ICJECE.2020.3018495.

[20] S. Purushothaman, D. Samiappan, M. Kamalkannan, N. Joseph, and R. Murugavel, "LVRT Enhancement of DFIG-based WECS using SVPWM-based Inverter Control," *Recent Advances in Electrical & Electronic Engineering*, vol. 17, no. 4, pp. 345-357, 2024, http://dx.doi.org/10.2174/2352096516666230606103013.

[21] I. R. de Oliveira, F. L. Tofoli, and V. F. Mendes, "Thermal analysis of power converters for DFIG-based wind energy conversion systems during voltage sags," *Energies*, vol. 15, no. 9, p. 3152, 2022, https://doi.org/10.3390/en15093152.

[22] L. Pan and C. Shao, "Wind energy conversion systems analysis of PMSG on offshore wind turbine using improved SMC and Extended State Observer," *Renewable Energy*, vol. 161, pp. 149-161, 2020, https://doi.org/10.1016/j.renene.2020.06.057.

[23] M. A. Mossa, O. Gam, N. Bianchi and N. V. Quynh, "Enhanced Control and Power Management for a Renewable Energy-Based Water Pumping System," *IEEE Access*, vol. 10, pp. 36028-36056, 2022, https://doi.org/10.1109/ACCESS.2022.3163530.

[24] M. M. Islam and D. Chowdhury, "Advanced and comprehensive control methods in wind energy systems," *CRC Press*, pp. 191-224, 2021, https://doi.org/10.1201/9781003058472-6.

[25] M. K. K. Prince, M. T. Arif, A. Gargoom, A. M. T. Oo and M. E. Haque, "Modeling, Parameter Measurement, and Control of PMSG-based Grid-connected Wind Energy Conversion System," *Journal of Modern Power Systems and Clean Energy*, vol. 9, no. 5, pp. 1054-1065, 2021, https://doi.org/10.35833/MPCE.2020.000601.

[26] A. M. I. Mohamad, M. Fakhari Moghaddam Arani and Y. A. -R. I. Mohamed, "Investigation of Impacts of Wind Source Dynamics and Stability Options in DC Power Systems With Wind Energy Conversion Systems," *IEEE Access*, vol. 8, pp. 18270-18283, 2020, https://doi.org/10.1109/ACCESS.2020.2966363.

[27] K. Palanimuthu, G. Mayilsamy, S. R. Lee, S. Y. Jung, and Y. H. Joo, "Comparative analysis of maximum power extraction and control methods between PMSG and PMVG-based wind turbine systems,"

International Journal of Electrical Power & Energy Systems, vol. 143, p. 108475, 2022, https://doi.org/10.1016/j.ijepes.2022.108475.

[28] E. C. Navarrete, M. Trejo Perea, J. C. Jáuregui Correa, R. V. Carrillo Serrano and G. J. R. Moreno, "Expert Control Systems Implemented in a Pitch Control of Wind Turbine: A Review," *IEEE Access*, vol. 7, pp. 13241-13259, 2019, https://doi.org/10.1109/ACCESS.2019.2892728.

[29] S. Foti, A. Testa, S. De Caro, L. D. Tornello, G. Scelba, and M. Cacciato, "Multi-level multi-input converter for hybrid renewable energy generators," *Energies*, vol. 14, no. 6, p. 1764, 2021, https://doi.org/10.3390/en14061764.

[30] Y. Gang, G. Yichang, Z. Lidan, L. Dongdong and L. Xing, "Multi-Phase Permanent Magnet Synchronous Generator Variable Speed Constant Frequency Offshore Wind System Based on Modular Multilevel Converter," *2019 IEEE Innovative Smart Grid Technologies - Asia (ISGT Asia)*, pp. 2127-2132, 2019, https://doi.org/10.1109/ISGT-Asia.2019.8881506.

[31] M. A. Mossa, N. Vu Quynh, H. Echeikh, and T. D. Do, "Deadbeat-Based Model Predictive Voltage Control for a Sensorless Five-Phase Induction Motor Drive," *Mathematical Problems in EngineeringMathematical Problems in Engineering*, vol. 2020, no. 1, pp. 1-30, 2020, https://doi.org/10.1155/2020/4164526.

[32] M. A. Mossa, H. Echeikh, A. A. Z. Diab, H. Haes Alhelou, and P. Siano, "Comparative study of hysteresis controller, resonant controller and direct torque control of five-phase IM under open-phase fault operation," *Energies*, vol. 14, no. 5, p. 1317, 2021, https://doi.org/10.3390/en14051317.

[33] G. Li, J. Hu, Y. Li and J. Zhu, "An Improved Model Predictive Direct Torque Control Strategy for Reducing Harmonic Currents and Torque Ripples of Five-Phase Permanent Magnet Synchronous Motors," *IEEE Transactions on Industrial Electronics*, vol. 66, no. 8, pp. 5820-5829, 2019, https://doi.org/10.1109/TIE.2018.2870359.

[34] A. Khamitov and E. L. Severson, "Design of Multi-Phase Combined Windings for Bearingless Machines," *IEEE Transactions on Industry Applications*, vol. 59, no. 3, pp. 3243-3255, 2023, https://doi.org/10.1109/TIA.2023.3243595.

[35] N. Mohamed, D. Abdelkader, and B. Y. Mohammed, "Modeling of Two Five-Phase Induction Machines Connected in Series with an Open Phase," *Advanced Computational Techniques for Renewable Energy Systems*, pp. 555-564, 2022, https://doi.org/10.1007/978-3-031-21216-1_57.

[36] O. Stiscia, M. Biasion, S. Rubino, S. Vaschetto, A. Tenconi and A. Cavagnino, "Iron Losses and Parameters Investigation of Multi-Three-Phase Induction Motors in Normal and Open-Phase Fault Conditions," *2022 International Conference on Electrical Machines (ICEM)*, pp. 793-799, 2022, https://doi.org/10.1109/ICEM51905.2022.9910784.

[37] J. Kellner and M. Praženica, "Research into the possibility of improving the efficiency and torque ripple of a drive with a five-phase induction motor by Changing the control in a fault state," *2022 International Symposium on Power Electronics, Electrical Drives, Automation and Motion (SPEEDAM)*, pp. 663-670, 2022, https://doi.org/10.1109/SPEEDAM53979.2022.9842124.

[38] H. T. Canseven and A. Ünsal, "Performance Improvement of a Five-Phase PMSM Drive Under Open Circuit Stator Faults," *2021 5th International Symposium on Multidisciplinary Studies and Innovative Technologies (ISMSIT)*, pp. 561-565, 2021, https://doi.org/10.1109/ISMSIT52890.2021.9604537.

[39] R. Basak, G. Bhuvaneswari and R. R. Pillai, "Low-Voltage Ride-Through of a Synchronous Generator-Based Variable Speed Grid-Interfaced Wind Energy Conversion System," *IEEE Transactions on Industry Applications*, vol. 56, no. 1, pp. 752-762, 2020, https://doi.org/10.1109/TIA.2019.2946125.

[40] S. Rhaili, A. Abbou, S. Marhraoui, N. El Hichami and A. V. Hemeyine, "Robustness investigation of Vector Control of Five-phase PMSG based Variable-Speed Wind Turbine under faulty condition," *2018 Renewable Energies, Power Systems & Green Inclusive Economy (REPS-GIE)*, pp. 1-6, 2018, https://doi.org/10.1109/REPSGIE.2018.8488809.

[41] M. R. M. Hassan, M. Mossa, and G. M. Dousoky, "Dynamic Performance Analysis of An Electric Vehicle System Using Different Control Algorithms," *Journal of Advanced Engineering Trends*, vol. 43, no. 1, pp. 151-162, 2024, https://dx.doi.org/10.21608/jaet.2022.138420.1202.

[42] C. S. T. Dong, H. H. Le, and H. H. Vo, "Field oriented controlled permanent magnet synchronous motor drive for an electric vehicle," *International Journal of Power Electronics and Drive Systems*, vol. 14, no. 3, pp. 1374-1381, 2023, http://doi.org/10.11591/ijpeds.v14.i3.pp1374-1381.

[43] A. Benevieri, L. Carbone, S. Cosso, F. Gallione, D. Gnudi and S. Hussain, "Field Oriented Control System Modeling for a New Flywheel Energy Storage System," *2023 13th International Symposium on Advanced Topics in Electrical Engineering (ATEE)*, pp. 1-7, 2023, https://doi.org/10.1109/ATEE58038.2023.10108380.

[44] B. G. Ranjolkar, S. Angadi and A. B. Raju, "Field Oriented Control of Synchronous Reluctance Machine for Electric Vehicle Applications," *2022 IEEE North Karnataka Subsection Flagship International Conference (NKCon)*, pp. 1-5, 2022, https://doi.org/10.1109/NKCon56289.2022.10126850.

[45] A. Dieng, J. C. Le Claire, A. B. Mboup, M. F. Benkhoris and M. Aït-Ahmed, "An improved torque control strategy of "five-phase PMSG-PWM rectifier" set for marine current turbine applications," *2019 IEEE 13th International Conference on Compatibility, Power Electronics and Power Engineering (CPE-POWERENG)*, pp. 1-6, 2019, https://doi.org/10.1109/CPE.2019.8862372.

[46] P. Colli and D. Manini, "Sliding mode control for a generalization of the Caginalp phase-field system," *Applied Mathematics & Optimization*, vol. 84, pp. 1395-1433, 2021, https://doi.org/10.1007/s00245-020-09682-3.

[47] A. Ma'arif, M. A. M. Vera, M. S. Mahmoud, E. Umoh, A. J. Abougarair, and S. N. Rahmadhia, "Sliding Mode Control Design for Magnetic Levitation System," *Journal of Robotics and Control*, vol. 3, no. 6, pp. 848-853, 2022, https://doi.org/10.18196/jrc.v3i6.12389.

[48] R. Rahmatullah, A. Ak, and N. F. O. Serteller, "SMC controller design for DC motor speed control applications and performance comparison with FLC, PID and PI controllers," *Intelligent Sustainable Systems*, vol. 579, pp. 607-617, 2023, https://doi.org/10.1007/978-981-19-7663-6_57.

[49] O. Dange, N. Patil, S. Gadgune and R. M. Linus, "Speed Control of BLDC Motor using Integral Sliding Mode Controller," *2023 Third International Conference on Advances in Electrical, Computing, Communication and Sustainable Technologies (ICAECT)*, pp. 1-4, 2023, https://doi.org/10.1109/ICAECT57570.2023.10117574.

[50] S. Chen, G. Wu, and C. Yu, "Robust fractional-order integral terminal sliding mode control with adaptive uncertainty observation for a VCM-driven X–Y motion stage," *IET Electric Power Applications*, vol. 17, no. 2, pp. 161-180, 2023, https://doi.org/10.1049/elp2.12252.

[51] A. Rajeevan and L. P. P. S, "Higher Order Integral Sliding Mode Controller for a Robotic Manipulator," *IECON 2022 – 48th Annual Conference of the IEEE Industrial Electronics Society*, pp. 1-6, 2022, https://doi.org/10.1109/IECON49645.2022.9968410.

[52] M. R. M. Hassan, M. A. Mossa, and G. M. Dousoky, "Evaluation of electric dynamic performance of an electric vehicle system using different control techniques," *Electronics*, vol. 10, no. 21, p. 2586, 2021, https://doi.org/10.3390/electronics10212586.

[53] V. Yaramasu and B. Wu, "Model predictive control of wind energy conversion systems," *John Wiley & Sons*, 2016, https://doi.org/10.1002/9781119082989.

[54] A. A. Ahmed, A. Bakeer, H. H. Alhelou, P. Siano, and M. A. Mossa, "A new modulated finite control set-model predictive control of quasi-Z-source inverter for PMSM drives," *Electronics*, vol. 10, no. 22, p. 2814, 2021, https://doi.org/10.3390/electronics10222814.

[55] Z. Zhang, Z. Li, M. P. Kazmierkowski, J. Rodríguez and R. Kennel, "Robust Predictive Control of Three-Level NPC Back-to-Back Power Converter PMSG Wind Turbine Systems With Revised Predictions," *IEEE Transactions on Power Electronics*, vol. 33, no. 11, pp. 9588-9598, 2018, https://doi.org/10.1109/TPEL.2018.2796093.

[56] Z. Zhang, H. Fang, F. Gao, J. Rodríguez and R. Kennel, "Multiple-Vector Model Predictive Power Control for Grid-Tied Wind Turbine System With Enhanced Steady-State Control Performance," *IEEE Transactions on Industrial Electronics*, vol. 64, no. 8, pp. 6287-6298, 2017, https://doi.org/10.1109/TIE.2017.2682000.

[57] M. A. Mossa and S. Bolognani, "Predictive Power Control for a Linearized Doubly Fed Induction Generator Model," *2019 21st International Middle East Power Systems Conference (MEPCON)*, pp. 250-257, 2019, https://doi.org/10.1109/MEPCON47431.2019.9008085.

[58] I. Jlassi and A. J. Marques Cardoso, "Enhanced and Computationally Efficient Model Predictive Flux and Power Control of PMSG Drives for Wind Turbine Applications," *IEEE Transactions on Industrial Electronics*, vol. 68, no. 8, pp. 6574-6583, 2021, https://doi.org/10.1109/TIE.2020.3005095.

[59] P. R. U. Guazzelli, W. C. de Andrade Pereira, C. M. R. de Oliveira, A. G. de Castro and M. L. de Aguiar, "Weighting Factors Optimization of Predictive Torque Control of Induction Motor by Multiobjective Genetic Algorithm," *IEEE Transactions on Power Electronics*, vol. 34, no. 7, pp. 6628-6638, 2019, https://doi.org/10.1109/TPEL.2018.2834304.

[60] M. A. Mossa, O. Gam, and N. Bianchi, "Dynamic performance enhancement of a renewable energy system for grid connection and stand-alone operation with battery storage," *Energies*, vol. 15, no. 3, p. 1002, 2022, https://doi.org/10.3390/en15031002.

[61] M. E. Emna, K. Adel, and M. F. Mimouni, "The wind energy conversion system using PMSG controlled by vector control and SMC strategies*," International journal of renewable energy research*, vol. 3, no. 1, pp. 41-50, 2013, https://dergipark.org.tr/en/pub/ijrer/issue/16080/168268.

[62] L. Shengquan, L. Juan, T. Yongwei, S. Yanqiu, and C. Wei, "Model-based model predictive control for a direct-driven permanent magnet synchronous generator with internal and external disturbances," *Transactions of the Institute of Measurement and Control*, vol. 42, no. 3, pp. 586-597, 2020, https://doi.org/10.1177/0142331219878574.

[63] G. Mayilsamy *et al*., "A Review of State Estimation Techniques for Grid-Connected PMSG-Based Wind Turbine Systems," *Energies*, vol. 16, no. 2, p. 634, 2023, https://doi.org/10.3390/en16020634.

[64] Z. Jamal Mohammed, S. Enad Mohammed and M. Obaid Mustafa, "Improving the Performance of Pitch Angle Control of Variable Speed Wind Energy Conversion Systems Using Fractional PI Controller," *2022 Iraqi International Conference on Communication and Information Technologies (IICCIT)*, pp. 209-215, 2022, https://doi.org/10.1109/IICCIT55816.2022.10010639.

[65] A. Mansouri, I. e. Myasse, A. E. Magri, R. Lajouad and F. Giri, "Nonlinear Control of Five-Phase PMSG Wind Turbine connected to Vienna Type Rectifier Using SVPWM," *2023 3rd International Conference on Innovative Research in Applied Science, Engineering and Technology (IRASET)*, pp. 1-6, 2023, https://doi.org/10.1109/IRASET57153.2023.10152932.

[66] M. A. Mossa and S. Bolognani, "Effective model predictive direct torque control for an induction motor drive," *2016 International Symposium on Power Electronics, Electrical Drives, Automation and Motion (SPEEDAM)*, pp. 746-754, 2016, https://doi.org/10.1109/SPEEDAM.2016.7525814.

[67] D. Zheng, G. Lu, Y. Yang, Q. Zhang and P. Zhang, "The Online Stator Winding Insulation Monitoring for PMSG-PWM rectifier System under Various Working Conditions," *IECON 2021 – 47th Annual Conference of the IEEE Industrial Electronics Society*, pp. 1-6, 2021, https://doi.org/10.1109/IECON48115.2021.9589591.

[68] M. A. Mossa and S. Bolognani, "Effective model predictive direct torque control for an induction motor drive," *2016 International Symposium on Power Electronics, Electrical Drives, Automation and Motion (SPEEDAM)*, pp. 746-754, 2016, https://doi.org/10.1109/SPEEDAM.2016.7525814.

[69] M. R. Hazari, E. Jahan, M. A. Mannan, and N. Das, "Transient stability enhancement of a grid-connected large-scale PV system using fuzzy logic controller," *Electronics*, vol. 10, no. 19, p. 2437, 2021, https://doi.org/10.3390/electronics10192437.

[70] A. Memon, M. W. Mustafa, M. N. Aman, A. Hafeez, and M. Ullah, "Improving transient behavior of a brushless doubly fed induction generator through reactive current control of grid-side converter," *Electronics*, vol. 10, no. 12, p. 1413, 2021, https://doi.org/10.3390/electronics10121413.

[71] X. Kong, X. Liu, L. Ma and K. Y. Lee, "Hierarchical Distributed Model Predictive Control of Standalone Wind/Solar/Battery Power System," *IEEE Transactions on Systems, Man, and Cybernetics: Systems*, vol. 49, no. 8, pp. 1570-1581, 2019, https://doi.org/10.1109/TSMC.2019.2897646.

[72] I. Jlassi and A. J. Marques Cardoso, "Open-circuit fault-tolerant operation of permanent magnet synchronous generator drives for wind turbine systems using a computationally efficient model predictive current control," *IET Electric Power Applications*, vol. 15, no. 7, pp. 837-846, 2021, https://doi.org/10.1049/elp2.12062.